AGU ADVANCING EARTH AND SPACE SCIENCES

Earth and Space Science

RESEARCH ARTICLE
10.1029/2023EA003119

A Theory of Maximum Entropy Production and Its Application to Microwave Remote Sensing—Simultaneous Retrieval of Soil Moisture and Vegetation Water Content

J. Wang[1], K. Cho[1], R. I. Negron-Juarez[2], A. Colliander[3], E. C. Caravasi[4], and N. S. Revilla[4]

[1]School of Civil and Environmental Engineering, Georgia Institute of Technology, Atlanta, GA, USA, [2]Climate and Ecosystem Sciences Division, Lawrence Berkeley National Laboratory, Berkeley, CA, USA, [3]Jet Propulsion Laboratory, California Institute of Technology, Pasadena, CA, USA, [4]Pontifical Catholic University of Peru, Lima, Peru

Abstract A theory of maximum entropy production (MEP) for electromagnetic wave propagation in dielectric materials is proposed and applied to simultaneously retrieving soil moisture (SM) and vegetation water content (VWC) from L-band microwave brightness temperature (TB). One representation of the MEP principle states that a non-equilibrium system corresponds to such a configuration of energy fluxes that minimizes a dissipation function under the constraint of energy conservation. The dissipation function for radiative transfer is formulated as an analogy of that for heat transfer. A new physical parameter, radiative inertia as an analogy of thermal inertia, is introduced to characterize radiative attenuation in dielectric media. The radiative inertia is parameterized in terms of the penetration depth of electromagnetic waves as a function of the complex dielectric constant. The MEP based retrieval algorithm predicts SM and VWC by minimizing the dissipation function under the constraint of the conservation of radiative energy. The retrievals of SM and VWC based on the MEP theory were validated against field observations in tropical and temperate forested regions of the Amazon and North America. The proof-of-concept analysis demonstrates the capability of the MEP algorithm for simultaneous retrievals of SM and VWC even for dense canopy (e.g., VWC > 5 kg m^{-2}). The MEP method is a new theoretical framework for developing innovative remote sensing algorithms of the Earth system not limited to microwave observations.

Plain Language Summary Satellite remote sensing using microwave radiometers provides global soil moisture data for studying the Earth's water, energy, and carbon cycles. However, measuring soil moisture over areas with dense canopy covering about 30% of global land can be challenging due to the attenuation of microwave signals through plants. Currently available soil moisture products offer reliable retrievals of soil moisture only for the areas of low to moderate vegetation water content (less than 5 kg m^{-2}). We developed a novel algorithm based on a new theory of radiative transfer that can help the development of soil moisture product for areas with dense canopy, such as tropical and temperate forests with high vegetation water content. The algorithm uses satellite observations of microwave brightness temperature, surface temperature, and vegetation and soil physical parameters. Initial validation of the proposed theory and algorithm yields promising results.

Key Points:

- A theory of maximum entropy production (MEP) for radiative transfer in dielectric materials is proposed and applied to L-band microwave brightness temperature remote sensing data
- Simultaneous retrievals of soil moisture and vegetation water content combined with physical temperature of canopy and soil are possible using the MEP method
- The proposed methodology produced satisfactory results even for dense forests

Supporting Information:

Supporting Information may be found in the online version of this article.

Correspondence to:

J. Wang,
jingfeng.wang@ce.gatech.edu

Citation:

Wang, J., Cho, K., Negron-Juarez, R. I., Colliander, A., Caravasi, E. C., & Revilla, N. S. (2024). A theory of maximum entropy production and its application to microwave remote sensing—Simultaneous retrieval of soil moisture and vegetation water content. *Earth and Space Science*, *11*, e2023EA003119. https://doi.org/10.1029/2023EA003119

Received 19 JULY 2023
Accepted 13 FEB 2024

Author Contributions:

Conceptualization: J. Wang
Data curation: R. I. Negron-Juarez, E. C. Caravasi, N. S. Revilla
Formal analysis: J. Wang, K. Cho
Funding acquisition: J. Wang, R. I. Negron-Juarez, A. Colliander
Investigation: K. Cho
Methodology: J. Wang

1. Introduction

Global remote sensing data of soil moisture (SM) have been available from the Soil Moisture and Ocean Salinity (SMOS) mission since 2009 by the European Space Agency (ESA) (Kerr et al., 2010) and the Soil Moisture Active Passive (SMAP) mission since 2015 by the National Aeronautics and Space Administration (NASA) (Entekhabi et al., 2010). The SMOS and SMAP satellites measure dual polarization L-band (1.4 GHz) microwave brightness temperature (TB) at approximately 40 km resolution for the retrieval of surface (top 5 cm) SM. The two missions use similar retrieval algorithms for SM (Chan et al., 2016; Kerr et al., 2012; O'Neill, Bindlish, et al., 2020); hence face similar challenges in the retrieval of SM over densely vegetated areas covering ~30% of the global land surface (Chan et al., 2013).

Dense vegetation poses a major obstacle to the retrieval of SM due to a reduction in the sensitivity of TB to SM caused by vegetation water content (VWC). The sensitivity of L-band TB to SM for 5 kg m^{-2} VWC was shown to be 70% lower than that of bare soil (Jackson, 1993; Njoku & Entekhabi, 1996). VWC of 5 kg m^{-2}

Project administration: J. Wang, R. I. Negron-Juarez, A. Colliander
Resources: J. Wang, R. I. Negron-Juarez, A. Colliander
Supervision: J. Wang, R. I. Negron-Juarez, A. Colliander
Validation: J. Wang, K. Cho
Visualization: K. Cho
Writing – original draft: J. Wang
Writing – review & editing: J. Wang, K. Cho, R. I. Negron-Juarez, A. Colliander

corresponds roughly to full-grown corn. The SMAP SM data using the current single polarization retrieval algorithms (O'Neill et al., 2021; O'Neill, Bindlish, et al., 2020) have uncertain quality for VWC and no SM retrievals are made for VWC >30 kg m^{-2}. The original mission requirement called SM retrievals for areas with VWC less than 5 kg m^{-2} and the lack of validation data in areas with VWC more than 5 kg m^{-2} has impended the development of retrievals for these areas. About 30% of land surfaces are covered with either evergreen or deciduous broadleaf/needleleaf forests with VWC ~6–20 kg m^{-2} (Aviabile et al., 2016; Chan et al., 2013), the SM data provided by SMAP (and SMOS) are not reliable for these areas. For example, the SMAP SM products for the Amazon regions are severely biased (Cho et al., 2024). Improvement of SM retrieval for the regions covered with forest (VWC >5 kg m^{-2}) is one of the priority issues considered during the extended SMAP mission (O'Neill, Chan, et al., 2020; Colliander et al., 2022a, 2022b). Several recent efforts on SM retrieval for forested regions of high VWC (>5 kg m^{-2}) (Ayres et al., 2021; Colliander et al., 2020; Vittucci et al., 2016) indicate that the retrieval is possible. One proposed approach for assisting the retrieval of SM under a dense canopy is the hybrid method for the full wave simulations of 3D Maxwell equations applied to trees (Colliander et al., 2018; Gu et al., 2022; Jeong et al., 2023). The canopy transmissivities obtained from direct simulations of the Maxwell equations are much greater than those obtained from the traditional formulation of the radiative transfer equation, further suggesting the possibility of SM retrieval for dense canopy covered areas.

The SMAP baseline SM data are produced using the Dual Channel Algorithm (DCA) (O'Neill, Bindlish, et al., 2020). The retrievals of SM under the canopy are based on the tau-omega model (Jackson & Schmugge, 1991; Mo et al., 1982) to describe the transfer of microwave radiation of soil and canopy source. In addition to vertically (V)- and horizontally (H)-polarized TB, the SMAP DCA requires several model parameters provided by ancillary data, including canopy/soil temperature, single scattering albedo and surface roughness (Chaubell et al., 2022; O'Neill et al., 2021). The modeled V- and H-polarized TB are obtained based on the tau-omega model of radiative transfer in the Single Channel Algorithm (SCA) with different values of model parameters. The SCA for under-canopy SM retrieval has five steps (O'Neill, Bindlish, et al., 2020; O'Neill, Chan, et al., 2020): (a) calculating the "apparent emissivity" as the ratio of brightness temperature to soil/canopy surface temperature (assumed to be identical), (b) removing the effect of VWC based on the tau-omega model, (c) calculating soil emissivity accounting for the effect of surface roughness, (d) deriving the dielectric constant from the smooth (moist) soil emissivity according to the Fresnel equation, and (e) calculating soil moisture using dielectric mixing model(s). The ancillary data of soil temperature are from GSFC GMAO GEOS-FP outputs (SMAP Algorithm Development Team, 2015). Since both SMAP and SMOS satellites have sun-synchronized orbits with 6a.m./6p.m. equatorial overpass times, the canopy temperature profiles are close to the maximum uniformity at 6a.m. (O'Neill, Bindlish, et al., 2020; O'Neill, Chan, et al., 2020). The ancillary data of VWC are obtained from the combination of the Normalized Difference Vegetation Index (NDVI) based estimates of foliage water content and the Leaf Area Index (LAI) based estimates of stem water content (Chan et al., 2013). Other algorithm parameters such as surface roughness, the single scattering albedo of vegetation (omega), and the empirical coefficient (b) of vegetation optical depth (tau or VOD)—VWC relationship (e.g., Jackson & Schmugge, 1991) are provided by the land cover-driven lookup table. Among these algorithm parameters, the bias and uncertainty of the VOD from the ancillary data of VWC and the b coefficient have a strong impact on the accuracy of soil moisture retrievals through the tau-omega model.

The objective of this study is to develop a new method for retrieving SM under vegetation from L-band TB including dense canopy. This goal is achieved by formulating a novel algorithm of simultaneous retrievals of SM and VWC built on a newly proposed theory for the electromagnetic wave propagation in dielectric materials as the generalized theory of maximum entropy production (MEP) for heat transfer (Wang & Bras, 2009, 2011). The MEP algorithm is used to partition TB into two components of vegetation and soil source to obtain a simultaneous solution of soil emissivity and VWC. SM is then obtained from the retrieved soil emissivity using a dielectric mixing model (e.g., Dobson et al., 1985; Mironov et al., 2009; Wang & Schmugge, 1980). VWC is directly calculated using a parameterization of VOD—VWC relationship. The MEP algorithm represents vegetation using physical parameters of heat capacity and complex dielectric constant of liquid water, dry soil, and dry plant. This is the first proof-of-concept study of the MEP theory for the electromagnetic wave propagation and its application to the space-borne observation of SM under dense canopy, a long-standing challenge in the remote sensing of the Earth system.

2. Methods

2.1. MEP Theory

The MEP principle (Dewar, 2003, 2005) is a derivative of the principle of maximum entropy first proposed as an application of information theory in statistical mechanics (Jaynes, 1957) and now viewed as a general inference algorithm (Jaynes, 2003) applicable to physical systems including non-equilibrium thermodynamic systems. The MEP principle was first applied to modeling global climatic dynamics (Paltridge, 1975) and has been generalized to broader fields (Kleidon & Lorenz, 2005), including land surface hydrology (Kleidon & Schymanski, 2008; Wang & Bras, 2009, 2011), bio-ecological systems (Juretic & Zupanovic, 2003; Kleidon et al., 2010; Kleidon & Fraedrich, 2005; Shipley, 2010), to name a few earlier studies. The MEP principle has multiple equivalent representations with well-defined physical meanings, including the principle of minimum dissipation and the principle of maximum entropy production. The physical basis of the MEP principle is the notion that non-equilibrium systems tend to evolve toward potential equilibrium states following the most effective path or to reach such a state as close to an equilibrium as possible allowed by the physical constraints (e.g., the conservation of energy). Therefore, the MEP principle can be interpreted equally well as an inference algorithm and a physical principle (Dewar & Maritan, 2013).

The MEP viewed as a physical principle for the purpose of this study, for example, the principle of minimum dissipation, has been applied to developing innovative models of turbulent and conductive heat fluxes at the Earth's surface. A prototype of the MEP models of heat fluxes is the non-gradient formula of conductive heat fluxes (Wang & Bras, 2009). Consider the problem of heat transfer in two infinite one-dimensional columns in contact with a heat source located at the interface. The partition of the heat flux from the source into the two columns can be obtained from the temperature distributions as the analytical solutions of the corresponding heat transfer equations. The MEP principle provides an alternative approach to the same analytical expressions of the heat fluxes without solving the heat transfer equations. Since the MEP theory is a (physical and/or inference) principle concerning the macroscopic behavior of a thermodynamic system, the formulation of a MEP model of heat fluxes is based on a "dissipation function" (or "entropy production function") without referring to the heat transfer equations. The dissipation function is expressed in terms of the heat fluxes as a mathematical analogy of the thermal dissipation produced by electric currents through conductors. The two heat fluxes can be obtained by minimizing the dissipation function under the constraint of energy conservation. This prototype of the MEP models paved the way for developing a non-gradient model of latent, sensible and ground heat flux over the land surface (Wang & Bras, 2011), which has been extended to all surface types including water, snow, and ice (Wang et al., 2014). The MEP model has been extensively validated and widely applied (e.g., El Sharif et al., 2019; Hajji et al., 2018, 2021; Isabelle et al., 2021; Jia et al., 2023; Jing & Wang, 2023; Nearing et al., 2012; Shanafield et al., 2015; Tang et al., 2021; Wang et al., 2017; Wang, Liu, & Shen, 2023; Xu et al., 2019, 2023; Yang et al., 2022; Yang & Wang, 2014).

The MEP principle for conductive and turbulent heat transfer (Wang & Bras, 2009, 2011), briefly overviewed above, alludes to a MEP principle for radiative transfer in dielectric materials. This is possible because the Ohm's law, a macroscopic description of electromagnetic wave propagation in conductive materials, has two equivalent representations in the forms of the principle of minimum dissipation and the principle of maximum entropy production (see Appendix A). The mathematical analogy between the thermal dissipation function of current through a conductor and the generalized dissipation function of heat transfer suggests that the MEP principle, in the form of the principle of minimum dissipation, may hold for radiative transfer in dielectric materials associated with a similar dissipation function. The physical analogy between them suggests that this newly introduced dissipation function characterizes the attenuation of electromagnetic waves in dielectric media. In this study, the proposed MEP principle for radiative transfer is validated by formulating an algorithm for the simultaneous retrieval of soil emissivity (and SM) and VWC from L-band TB observations.

2.2. Formulation of MEP Algorithms

The MEP algorithm for the retrieval of soil emissivity and VWC is formulated using the same method as that for formulating the MEP model of heat fluxes (Wang & Bras, 2009), that is, minimization of the dissipation function under the constraint of the conservation of (radiation) energy. For the radiative transfer in a canopy, the conservation of energy associated with the radiation flux received by a microwave radiometer is commonly represented by the tau-omega model (Jackson & Schmugge, 1991; Mo et al., 1982),

$$(1-\gamma)\left[1+(1-e_s)\gamma\right](1-\omega)\,T_v+\gamma e_s T_s=T_B \tag{1}$$

where T_B is the V- or H-polarized brightness temperature (K), T_v the canopy temperature (K), T_s the soil temperature (K), e_s the soil emissivity, γ the canopy transmissivity, and ω single scattering albedo of the canopy. For convenience, the two components on the left-hand-side of Equation 1 are written as the radiometer signals of canopy and soil source, respectively,

$$\begin{aligned} F_v &= (1-\gamma)\left[1+(1-e_s)\gamma\right](1-\omega)\,T_v \\ F_s &= \gamma e_s T_s \end{aligned} \tag{2}$$

where F_v and F_s are the L-band radiative flux from canopy and soil, respectively, received by the radiometer. A dissipation function D characterizing the loss of radiative energy of electromagnetic wave propagating in vegetation and soil medium into heat is postulated as an analogy of radiative transfer in conducting media to the conductive and turbulent heat transfer,

$$D(F_v,F_s)=\frac{F_v^2}{I_v+I_w}+\frac{F_s^2}{I_s+I_w} \tag{3}$$

where I_w,I_s,I_v are introduced new physical parameters, that is, the "radiative inertia" associated with the electromagnetic wave propagation in dielectric media of liquid water, dry soil and dry vegetation (the same value assumed for foliage and trunk), respectively,

$$\begin{aligned} I_w &= \rho_w c_w\sqrt{\kappa_w} \\ I_s &= \rho_s c_s\sqrt{\kappa_s} \\ I_v &= \rho_v c_v\sqrt{\kappa_v} \end{aligned} \tag{4}$$

with $\rho_w c_w$, $\rho_s c_s$, $\rho_v c_v$ are the heat capacity of (liquid) water, dry soil, and dry vegetation, respectively, and κ_w, κ_s, κ_v introduced as the "radiative diffusivity" of liquid water, dry soil and dry vegetation, respectively. The vegetation is assumed as uniform layer of constant dielectric properties. The diffusivity of radiative transfer, a non-gradient-based radiative energy transfer process, is parameterized as an analogy of gradient-based transport processes, such as conductive and turbulent heat transfer in soil and atmosphere (Jing & Wang, 2023),

$$\begin{aligned} \kappa_w &= \omega_0\delta_w^2 \\ \kappa_s &= \omega_0\delta_s^2 \\ \kappa_v &= \omega_0\delta_v^2 \end{aligned} \tag{5}$$

where ω_0 is the characteristic (e.g., diurnal or seasonal) angular frequency (i.e., time scales of the thermal effect of the microwave radiation) and δ_w, δ_s, δ_v are the wavelength-dependent e-fold penetration depth of electromagnetic wave in dielectric media of liquid water, dry soil and dry vegetation, respectively. The penetration depth δ is a function of complex dielectric constant $\varepsilon' - i\varepsilon''$ (e.g., Ulaby et al., 1982, p. 847)

$$\begin{aligned} \delta &= \frac{\lambda}{4\pi\left|\mathrm{Im}\sqrt{\varepsilon}\right|} \\ \mathrm{Im}\sqrt{\varepsilon} &= \left(\varepsilon'^2+\varepsilon''^2\right)^{\frac{1}{4}}\sin\left[\frac{1}{2}\tan^{-1}\left(\frac{\varepsilon''}{\varepsilon'}\right)\right]\approx\frac{\varepsilon''}{2\sqrt{\varepsilon'}}\ \text{for}\ \varepsilon'\gg\varepsilon'' \end{aligned} \tag{6}$$

where λ is the wavelength of microwave radiation (e.g., 21 cm at L-band 1.4 GHz). The complex dielectric constants and the resulting L-band penetration depths of liquid, dry soil, and dry vegetation are given in Table 1. The subscripts "w", "s", "v" refer to "water" "dry soil" and "dry vegetation," respectively. Representative values $\delta_w = 5$ cm, $\delta_s = 4$ m, $\delta_v = 1.5$ m are assumed in the validation of the MEP algorithms.

Table 1
Complex Dielectric Constants and L-Band (1.4 GHz) Penetration Depths in Equation 6

	Liquid water (w)[a]	dry soil (s)[b]	dry plant (v)[c]
ε'	~80	~2–7	~2–6
ε''	~10	≤0.05	~0.01–0.1
δ (cm)	~3–5	~100–500	~50–500

[a]Reul & Chapron, 2001. [b]Njoku & Kong, 1977; Ulaby et al., 1986; Zawislansji et al., 1997. [c]Torgovnikov, 1993.

Minimizing the dissipation function D in Equation 3 subject to the energy conservation constraint Equation 1,

$$\min_{\{F_v,F_s\}}\{D(F_v,F_s)|F_v+F_s=T_B\} \tag{7}$$

leads to the solution of F_s, F_v in terms of T_B, T_s, T_v,

$$F_s=\frac{T_B}{1+\sigma^{-1}},\qquad F_v=\frac{T_B}{1+\sigma},\qquad \sigma\equiv\frac{\rho_w c_w\delta_w+\rho_s c_s\delta_s}{\rho_w c_w\delta_w+\rho_v c_v\delta_v}. \tag{8}$$

The expressions of γ, e_s are obtained from Equations 2 and 8 for given ω,

$$\begin{aligned}\gamma&=\frac{A_s}{2}\left[1+\sqrt{1+\frac{4(1-A_s-A_v)}{A_s^2}}\right]\\ e_s&=\frac{A_s}{\gamma}\end{aligned}. \tag{9}$$

where A_s, A_v are analytical functions of brightness and physical temperature (T_B, T_s, T_v) and physical parameters of water, soil, and vegetation media ($\rho_w c_w\delta_w$, $\rho_s c_s\delta_s$, $\rho_v c_v\delta_v$),

$$\begin{aligned}A_v&\equiv\frac{1}{1+\sigma}\frac{T_B}{(1-\omega)T_v}\\ A_s&\equiv\frac{1}{1+\sigma^{-1}}\frac{T_B}{T_s}\end{aligned}. \tag{10}$$

It can be shown that $A_s+A_v\le 1$ under condition $(1-\omega)T_v\ge T_B$ guarantees physical solution $0\le\gamma\le 1$ and $0\le e_s\le 1$. Equation 9 is the MEP retrieval algorithm of canopy transmissivity and soil emissivity.

The physical parameters of the MEP algorithm are the radiative inertia defined in Equation 4. The radiative diffusivity defined in Equation 5 depends on the heat capacities and the penetration depths calculated from the complex dielectric constants of water, dry soil and dry vegetation according to Equation 6. The L-band penetration depth of liquid water is estimated as $\delta_w\sim 4$ cm (e.g., Reul & Chapron, 2001) depending on the salinity of vegetation water shown to be lower than ~1% (10 psu) (Liu et al., 2017; Mätzler, 1994; Xu et al., 2020). The penetration depth of dry soil may be estimated as $\delta_s\sim$ 100–500 cm or greater by extrapolating those as functions of soil moisture (Njoku & Entekhabi, 1996, Figure 4). The estimated penetration depth of dry vegetation $\delta_v\sim 50-500$ cm according to the estimated complex dielectric constant of dry leaves and trunks of various plants (El Rayes & Ulaby, 1987). The estimated penetration depths have uncertainties due largely to the uncertainty of the estimated imaginary part of the complex dielectric constants. In this study, the density of dry vegetation is taken as $\rho_v\sim 400$ kg m^{-3} (Shipley & Vu, 2002). The specific heat of dry vegetation is taken as 3×10^3 (the medium of its range of $1.5–5\times 10^3$) J ·kg^{-1} K^{-1} (Jayalakshmy & Philip, 2010).Only the representative values of these parameters will be used in this proof-of-concept analysis to show that the reasonable values of the physical parameters in the MEP algorithm will lead to realistic estimates of VWC and SM.

Canopy transmissivity γ is expressed in terms of the VOD τ,

$$\gamma=\exp\left(-\frac{\tau}{\cos\theta_0}\right), \tag{11}$$

where θ_0 is the surface incident angle of the radiometer and τ is related to VWC and dry vegetation (e.g., Jackson, 1993; Njoku, 2014; Njoku & Entekhabi, 1996),

$$\tau=\left(\frac{VWC}{\rho_w}\frac{1}{\delta_w}+\frac{M_v}{\rho_v}\frac{1}{\delta_v}\right)\approx\frac{VWC}{\rho_w\delta_w}, \tag{12}$$

where M_v is dry vegetation mass content (kg m^{-2}). Since $\delta_v \gg \delta_w$ (Table 1), VWC/ρ_w and M_v/ρ_v are comparable (e.g., Aviabile et al., 2016; Lu et al., 2022), VWC is obtained from Equations 11 and 12,

$$VWC = \rho_w \delta_w \cos\theta_0 \ln\frac{1}{\gamma} \tag{13}$$

where γ is the MEP solution in Equation 9, referred to as the MEP VWC retrieval algorithm.

The τ-VWC relationship is commonly expressed in an empirical (e.g., Jackson, 1993; Jackson & Schmugge, 1991) or semi-empirical (e.g., Njoku & Entekhabi, 1996; Wegmuller et al., 1995) equation $\tau = b \times VWC$ with vegetation structure dependent coefficient b. Equation 12 implies that b is a physical parameter,

$$b = \frac{1}{\rho_w \delta_w}. \tag{14}$$

Although b in general is assumed to account for the structural differences of different types of vegetation (Le Vine & Karam, 1996), the effect of the VWC on the attenuation of microwave radiation is represented here by, as a first approximation, the equivalent depth of VWC (i.e., uniformly spreading over the grid of SMAP L-band TB data ~9 km). This approximation is based on the fact that the large refractive index of water $n = \sqrt{\varepsilon_w} \sim 9$ ($\varepsilon_w \sim 80$ for liquid water) causes the microwave electromagnetic wave entering leaves nearly perpendicular to the leaf surface with the incident angle no more than 7° ($\sim sin^{-1}(1/n)$), hence justifies the expression of τ in Equation 12.

3. Data

Test of the MEP algorithms focuses on dense canopy since this type of forest represents a major challenge in remote sensing retrieval of VWC and SM. The selected sites in the Amazon and continental US are covered with either evergreen or deciduous broadleaf/needleleaf forest where field measurements of SM and other soil and meteorological data are available. Considering the uncertainties of the physical parameters in the MEP algorithms, especially the imaginary parts of dielectric constants of dry soil and dry vegetation, this proof-of-concept feasibility analysis aims to show that the MEP algorithms are able to produce realistic VWC and SM using reasonable estimates of these physical parameters.

The remote sensing data used in this proof-of-concept analysis are the SMAP L1C 6a.m. (LST) V-polarized at 9 km EASE2 grid resolution and GSFC GMAO GEOS-FP soil temperature (O'Neill et al., 2021) since V-polarized T_B leads to more accurate SMAP SM retrievals compared to the H-polarized T_B (Colliander et al., 2017) and canopy has on average a more uniform temperature profile ($T_s = T_v$) at 6 a.m. than at 6 p.m. The ancillary data of single scattering albedo of canopy layer (~0.07) are used when needed (Jackson & Schmugge, 1991; Njoku & Entekhabi, 1996). In situ data of SM for the validation of the MEP retrievals are from selected sites in the Amazon (Tambopata, Peru, [12.831°S, 69.283°W]) and the US (Missouri [38.744°S, 98.2°W] and New Hampshire [44.064°S, 71.287°W]). The Tambopata site in Peruvian Amazon is covered with dense and old-growth trees of average tree height 35 m and the tree density of 556 trees per hectare with a basal area of 25.9 square meters per hectare and average above-ground biomass (AGB) ~300 ton per hectare (Pallqui et al., 2014). The deciduous forest at the Missouri site has average tree height 22 m (Gu et al., 2016) and average ABG ~ 120 ton per hectare, and, and the deciduous forest at the New Hampshire site has average tree height 23 m and average ABG ~ 170 ton per hectare (Blackard et al., 2006). Site photos are provided in the Supporting Information (SI). Additional validation data are precipitation from Global Precipitation Measurement (GPM) IMERG (half-hourly, 10 km) (Huffman et al., 2019) and Enhanced Vegetation Index (EVI) (daily, 250 m) from MODIS Terra (Vermote & Wolfe, 2015).The three sites are located in tropical evergreen and temperate deciduous forest with high VWC (>5 kg m^{-2}) under which SM retrievals using the existing (e.g., SMOS, SMAP) algorithms have large biases. Direct validation of the MEP algorithm can be made by comparing the MEP retrievals of SM with in situ measurements available at the test sites. Since in situ measurements of VWC are not available, the MEP retrievals of VWC are evaluated against EVI data (as a surrogate of VWC) and the SMAP ancillary data for a consistency validation. The Amazon and the US have contrasting climate characterized by weak versus strong seasonality in temperature (Figure 1), respectively. Because TB depends on physical temperature, TB has similar seasonality to that of physical temperature (Figure 1). Even though the inputs of the MEP algorithm are brightness and physical

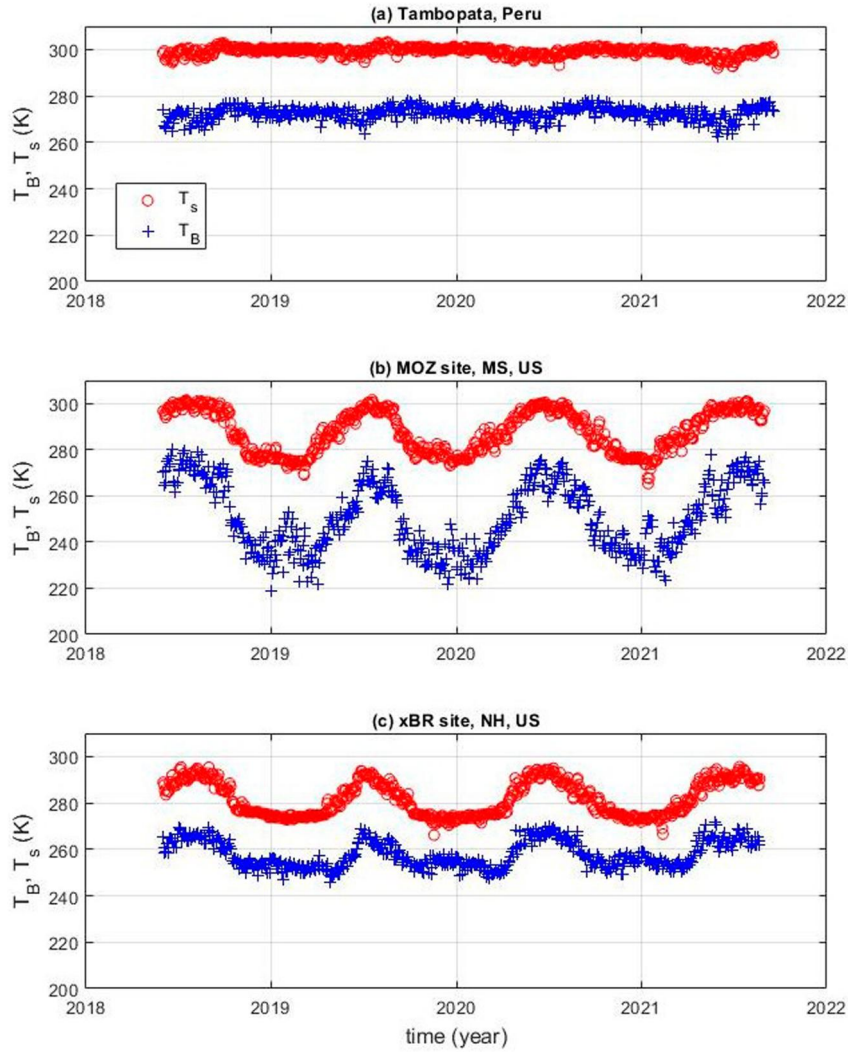

Figure 1. The inputs of the MEP algorithm: V-polarized L-band brightness temperature T_B and surface temperature T_s from the SMAP ancillary data. MS—Missouri, NH—New Hampshire.

temperature, the MEP retrievals of SM and VWC do not necessarily follow the same seasonality since SM is strongly affected by precipitation that may have different seasonality from that of soil temperature.

The MEP algorithm is also tested at three selected SMAP core validation sites with relatively low VWC (<5 kg m^{-2}) (Colliander et al., 2022) including Little Washita (34.97°N, 97.97°W) grassland in Oklahoma, Little River (31.64°N, 83.65°W) cropland/natural mosaic canopy in Georgia, and TxSON (30.5°N, 98.5°W) grassland in Texas. The SMAP core sites in situ data used in this study (Colliander et al., 2017) are available at https://nsidc.org/data/nsidc-0712. Daily 300 m fractional vegetation cover (FCOVER) data for the regions of the core validation sites are provided by Copernicus (Camacho et al., 2016). FCOVER data are derived from leaf area index and various canopy structure parameters based on remote sensing observations from the Sentinel-3 and PROBA satellites.

4. Validation of the MEP Algorithm

4.1. Results

Below we show the first proof-of-concept test of the MEP algorithm presented in Equations 9–13 for simultaneous retrieval of SM and VWC. The goal is to demonstrate the proposed algorithm with reasonable estimates of the physical parameters (i.e., dielectric constants and heat capacity) produces realistic SM and VWC. First, the

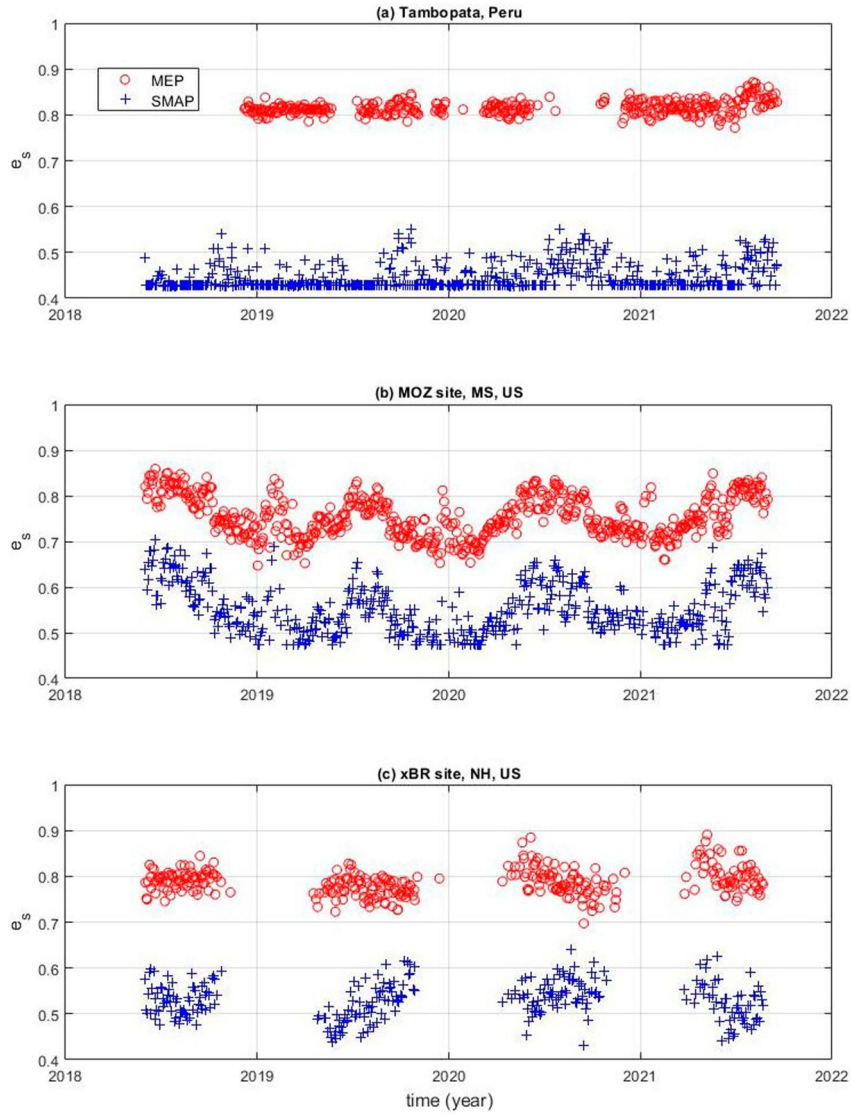

Figure 2. The MEP surface emissivity e_s in Equation 9 using the input data shown in Figure 1.

MEP solutions of soil emissivity e_s and canopy transmissivity γ are obtained from Equation 9. Then, VWC is obtained from Equation 13 using the MEP solution of γ. The MEP solution of e_s is used to calculate soil moisture using the dielectric mixing model used by the SMAP SCA (outlined Section 1).

The MEP retrievals of e_s and γ (Figures 2 and 3) from Equation 9 at the three sites clearly demonstrate different behaviors of the MEP algorithm in terms of non-linear functions of brightness and physical temperature (Figure 1). Since the MEP retrieval of e_s(Figure 2) cannot be directly validated (due to lack of in situ measurement), it is validated through the MEP retrieval of soil moisture (SM) (Figure 4). The current L-band TB based retrieval of SM is known to have large biases for the Amazon basin (Figure 4a) (e.g., Cho et al., 2024). The SMAP Level-3 Enhanced SM data (SPL3SMP_E, Version 5, https://nsidc.org/data/smap) for Tambopata site is mostly at saturation level, which is inconsistent with the in situ measurement of (surface) SM (Figure 4a). The MEP retrieval of SM using the MEP retrieval of e_s and SMAP SCA is consistent with the field measurements. In particular, the MEP algorithm captures the decreasing trend of SM at the end of observation period (June–September 2021) due to a drought associated with a La Niña event. SM at this site has weak seasonal variation even though rainfall has evident seasonality. This decrease in SM corresponds to the increasing trend of the MEP retrieval of e_s in Figure 2a. The agreement between the MEP retrieved and in situ SM demonstrates the feasibility of retrieving e_s with the MEP algorithm at dense forest sites. In this analysis, the systematic deviation of the MEP

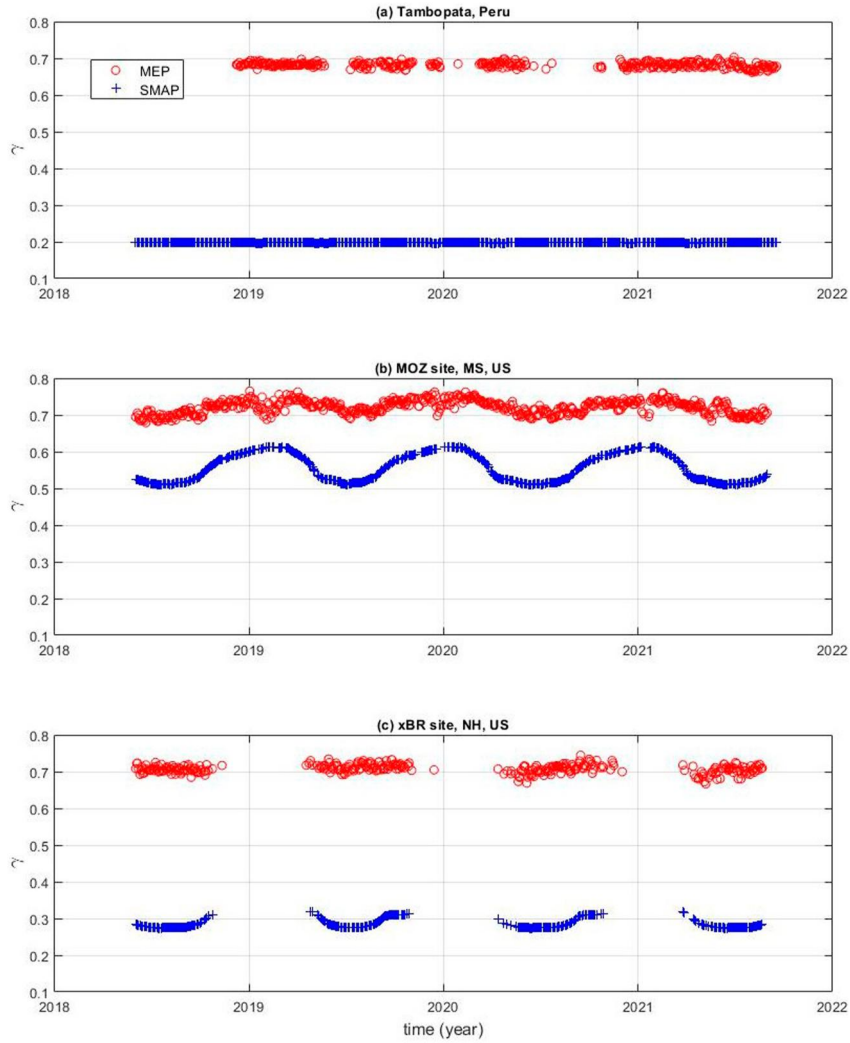

Figure 3. The MEP solution of canopy transmissivity γ in Equation 9 using the input data shown in Figure 1.

(SMAP) SM retrievals from (single site) in situ SM observations is represented by mean absolute difference (*MAD*), while the uncertainty and variability of the MEP (SMAP) SM retrievals relative to those of in situ SM by the root mean square variation of difference (*RMSVD*) and the correlation coefficient (*Corr*), respectively. For the Tambopata site, the statistics of the MEP (+SCA) versus in situ SM are MAD = 0.04, RMSVD = 0.06, Corr = 0.60 (Table 2), while the statistics of the SMAP versus in situ SM are MAD = 0.30, RMSVD = 0.30, Corr = 0.61.

The MEP SM, the SMAP Level-3 Enhanced SM based on SCA and field observations at the Missouri site (Figure 4b) have the same seasonal variation. The MEP SM being consistently lower than the SMAP SM is consistent with higher MEP e_s (by ~0.2) than the SMAP e_s (Figure 2b). The deviation of the MEP SM from the in situ SM (MAD = 0.08) may be related to the scale difference of MEP SM retrieval at 9 km and point measurement of SM. The correlation of the MEP SM retrieval versus in situ SM (Corr = 0.74) is higher than that for the Tambopata site Corr = 0.60 (Figure 4a). Rainfall at this site has weak seasonality. Therefore, the seasonal variation of SM is dominated by seasonal variation of canopy transpiration driven by solar radiation (Negron-Juarez et al., 2007). At the New Hampshire site, the MEP SM are more consistent with the field observations (MAD = 0.02, RMSVD = 0.03, Corr = 0.46) than the SMAP Level-3 Enhanced SM data MAD = 0.17, RMSVD = 0.18, Corr = 0.26 through the entire test period (Figure 4c). The lower MEP SM (~0.25) with MEP $e_s \sim 0.8$ is in closer agreement with in situ SM data (Figure 4c) than the SMAP SM (0.3–0.5) with the SMAP $e_s \sim 0.5$. The fact that smaller seasonal variations of the MEP SM and e_s than those of the SMAP SM and e_s are

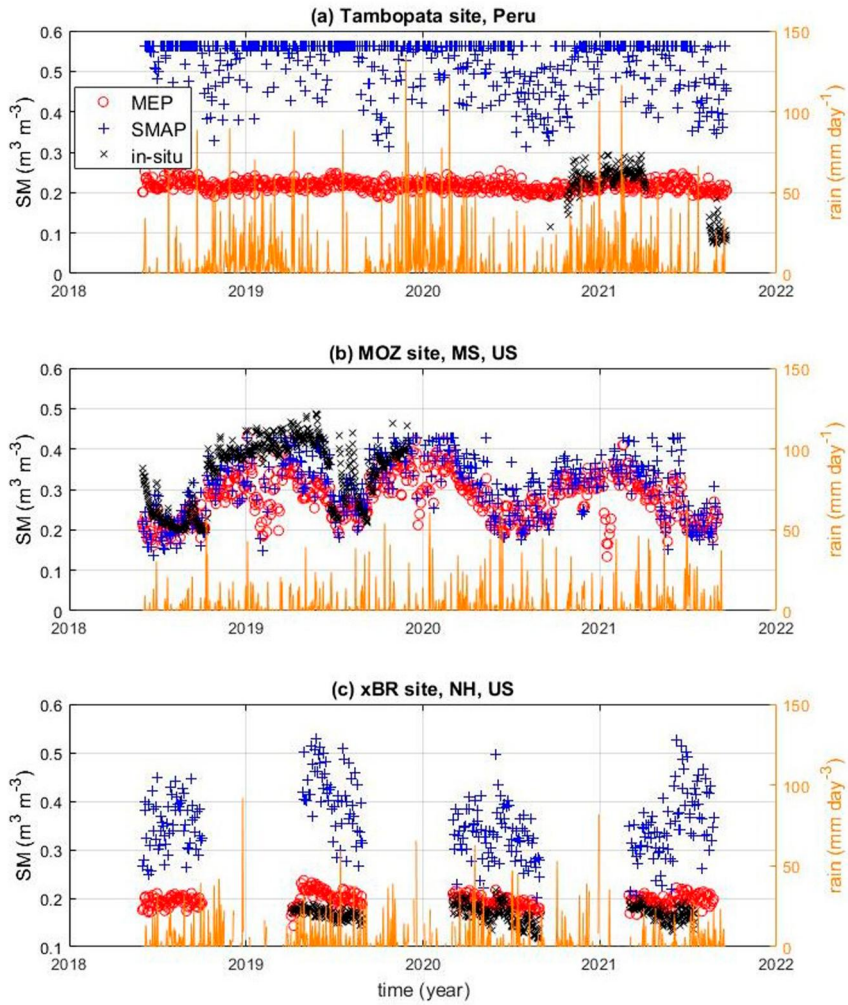

Figure 4. The MEP SM retrievals using the SMAP single channel algorithm (SCA) and the MEP e_s shown in Figure 2 versus SMAP and in situ SM data. The mean absolute difference (MAD) and root mean square variation of difference (RMSVD) and correlation coefficient (Corr) of the MEP retrievals relative to in situ SM data, respectively, in Table 2. Rainfall at (a) GPM IMERG, (b) 2018–2019 from AmeriFlux and 2020–2021 from GPM IMERG, (c) AmeriFlux.

Table 2
Statistics of MEP (+SCA) and SMAP Retrievals of SM (m^3 m^{-3}) Versus (Single Site) In-Situ Observations

	MEP versus OBS			SMAP versus OBS		
Site	MAD	RMSVD	Corr	MAD	RMSVD	Corr
Tambopata, Peru	0.04	0.06	0.60	0.30	0.30	0.61
MOZ (MS)	0.07	0.08	0.74	0.05	0.06	0.78
xBR (NH)	0.02	0.03	0.46	0.17	0.18	0.26
Little Washita (OK)	0.02	0.03	0.91	0.02	0.03	0.91
TxSON (TX)	0.02	0.04	0.88	0.02	0.03	0.88
LittleRiver (GA)	0.03	0.04	0.74	0.06	0.07	0.76

Note. *MAD*—mena absolute difference, *RMSVD*—root mean square variation of difference, *Corr*—correlation coefficient. MS—Missouri, NH—New Hampshire, OK—Oklahoma, TX—Texas, GA—Georgia.

more consistent with the in situ observations of SM and rainfall data (Figure 4c). For example, flat MEP and in situ SM during the summer of 2019 corresponding to rather uniform rainfall distribution while the SMAP SM showed obvious trends. Note that the MEP retrievals for the New Hampshire site are only shown for snow-free seasons (Figure 4c). The MEP algorithm for (frozen) soil moisture under snow cover is the topic of future research.

The MEP retrieval of γ (Figure 2) can be corroborated using the MEP retrievals of VWC. Since direct measurements of VWC at the three test sites are not available, the assessment of the MEP retrievals of VWC is through a consistency analysis using EVI data (as an indicator of canopy structure and state such as leaf area) and previously reported estimates of VWC. The MEP retrieved VWC for the Amazon site is ~12 kg m^{-2} with weak seasonality (Figure 5a) corresponding to $\gamma \sim 0.7$(Figure 3a), which is consistent with previously reported VWC for the Amazon region (e.g., Avitabile et al., 2016). The MEP algorithm also captures the weak intra-annual variability of VWC. In particular, the increasing MEP VWC during the dry season at the end of the

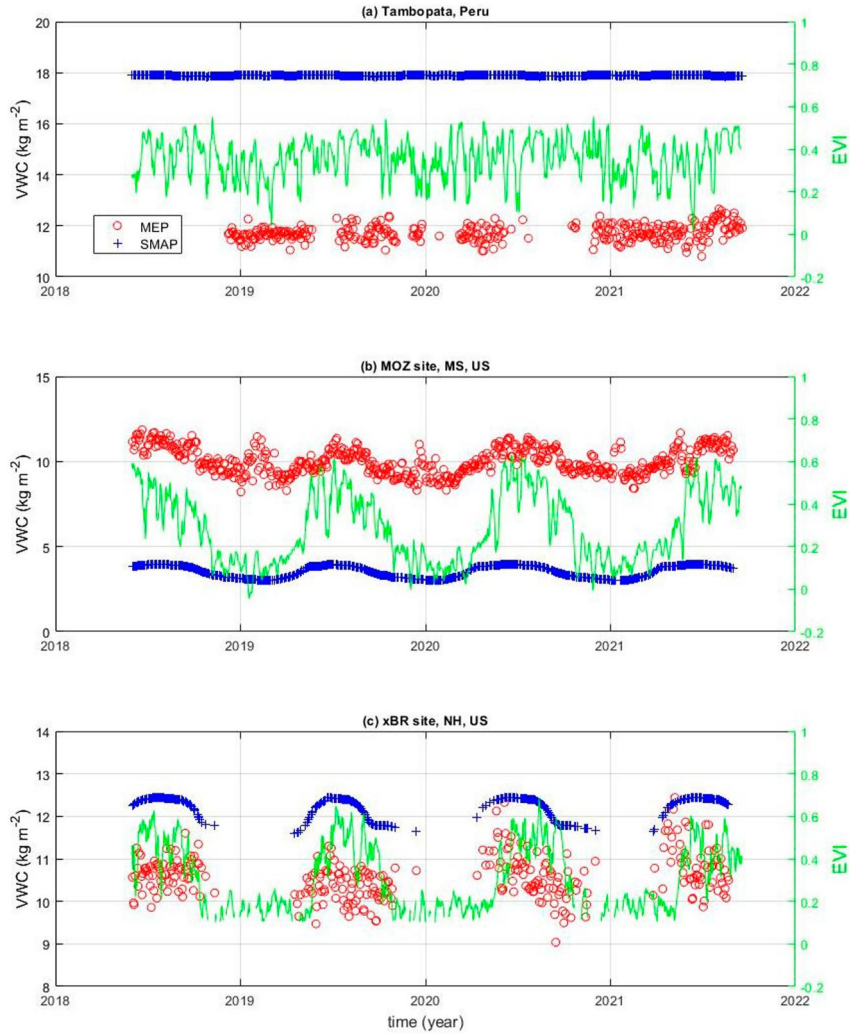

Figure 5. The MEP solution of vegetation water content VWC in Equation 13 derived from the MEP γ shown in Figure 3. The EVI data is 7-day moving average of the corresponding daily data.

study period in 2021 is likely caused by the green-up with sunlight in Amazon rainforests (Huete et al., 2006). This result is further confirmed by the EVI with a weak but apparent upward trend (Figure 5a) corresponding to the drying down of in situ SM (Figure 4a). The EVI over the entire period of 2018–2021 does not have pronounced seasonality even though the seasonality of rainfall at this Amazon site is evident (Figure 4a). In contrast, the SMAP ancillary data only show a constant climatology of VWC ($\sim$18 kg m^{-2}). The different magnitudes of the MEP and SMAP VWC are caused by the coefficient b in the expression of the vegetation optical depth $\tau = b \times VWC$. The SMAP default value of $b \sim 0.1$(O'Neill, Bindlish, et al., 2020) leads to $VWC \sim 18$ kg m^{-2} for $\gamma \sim 0.2$ or $\tau \sim 1.24$ (the SMAP ancillary data used in SCA), while $b \sim 0.025$ according to Equation 14 leads to $VWC \sim 12$ kg m^{-2} for the MEP retrieval of $\gamma \sim 0.7$ or $\tau \sim 0.3$ (Figure 3a). The SMAP DCA $\tau \sim 1.15$ corresponds to $VWC \sim 16$ kg m^{-2} for the same b($\sim$0.07) as that in the SCA assuming the DCA τ-VWC relationship is identical to that in the SCA even though a τ-VWC relationship has not established in the SMAP DCA. This is more consistent with the previously reported VWC ($\sim$15 kg m^{-2}) of the Amazon forest (Chan et al., 2013). The different estimates of VWC (SMAP SCA, DCA and MEP) are comparable within the range reported for the Amazon forest biomass (Avitabile et al., 2016). The Amazon forest VWC can be quantitatively evaluated once in situ observations of VWC become available. Detailed quantitative analysis is beyond scope of this study.

The MEP VWC for the Missouri site $\sim$10–11 kg m^{-2} are arguably more realistic than the corresponding SMAP VWC($<$5 kg m^{-2}) from ancillary data (Figure 5b) according to the documented VWC of deciduous forest (Chan

et al., 2013) (a site photo in SI). The low SMAP ancillary VWC for this site results from the equation $\tau = b \times VWC \sim 0.5$ while the MEP $\tau \sim 0.3$ supports the MEP algorithm of VWC in Equation 13 and the proposed formulation of b in $\tau = b \times VWC$ in Equation 14. Note that the MEP retrieval of VWC has stronger seasonal variation than that of the SMAP NDVI climatology-based VWC (Figure 5b) even though the seasonal variation of the MEP $\boldsymbol{\gamma}$ is weaker than that of the SMAP transmissivity based on the NDVI climatology-based VWC (SMAP ancillary) data (Figure 3b). The seasonal variation of TB (~50 K in Figure 1b) and the corresponding variation of VWC (~4 kg m^{-2}) at this site is much stronger than those of TB and VWC (~10 K in Figure 1a and ~1 kg m^{-2} in Figure 5a, respectively) at the Tambopata site. The pronounced seasonal variation of the MEP VWC retrievals is apparently correlated with strong seasonal cycle of EVI as an indicator of vegetation photosynthesis and biomass production (Sims et al., 2006). More quantitative analysis will be a topic of follow-up studies.

For the New Hampshire deciduous forest site, the MEP retrieved $VWC \sim$ 10–11 kg m^{-2} and SMAP NDVI climatology based $VWC \sim 12$ kg m^{-2} (Figure 5c), which are consistent with the documented VWC of deciduous forest (a site photo in SI) (Chan et al., 2013), are in much closer agreement than those at the Missouri site (Figure 5b). Yet, comparable MEP and NDVI climatology-based VWC associated with contrasting MEP $\boldsymbol{\gamma} \sim 0.7$ and SMAP $\boldsymbol{\gamma} \sim 0.3$ (Figure 3c) are again caused by the large difference in the corresponding b in $\tau = b \times VWC$. The greater variation of the MEP retrieved VWC during the growing season ~2 kg m^{-2} (Figure 5c) is more realistic than that of the NDVI climatology-based data <1 kg m^{-2} for deciduous forest. The seasonal variations of TB (~20 K and VWC ~2 kg m^{-2}, respectively) are consistent with those at the Tambopata (~10 K and VWC ~1 kg m^{-2}, respectively) and Missouri site (~50 K and VWC ~4 kg m^{-2}, respectively). This finding further supports the proposed formula in Equation 14. Note that the greater seasonal variation of the MEP retrieved VWC corresponds to smaller seasonal variation of the MEP retrieved $\boldsymbol{\gamma}$ versus the opposite behavior of the NDVI climatology-based VWC and γ (Figure 5c vs. Figure 3c). Our proof-of-concept analysis suggests that the MEP algorithm has the potential for detecting the seasonal variation of VWC from L-band TB.

The MEP algorithm provides consistent retrievals of SM and VWC for tropical evergreen and temperate deciduous forests covered regions. The validation analysis demonstrates the capability of the MEP algorithm for the retrieval of SM under dense canopy ($VWC >$ 5 kg m^{-2}). The MEP algorithm uses three input variables (i.e., brightness temperature, canopy and/or soil temperature) and includes only physical parameters (i.e., complex dielectric constant and heat capacity of liquid water, dry soil, and dry vegetation with fixed single scattering albedo) without referring to canopy structure characteristics.

The validation of the MEP algorithm against the field observations of SM at three SMAP core sites yields similar results (Figures 6–10) with the corresponding statistics in Table 2. The seasonality and magnitude of T_B, T_s at the core sites (Figure 6) are similar to those of the temperate forest sites (Figures 1b and 1c) except for higher sub-seasonal variations. The SMAP grids (33 km) where the three core sites are located have fractional vegetation cover f_c ranging from ~0.8 in summer to ~0.2 in winter (Figure S7 in Supporting Information S1). Soil emissivity under the (fractional) vegetation cover is calculated using the MEP algorithm in Equation 9, while soil emissivity without vegetation cover is directly obtained as T_B/T_s. The SMAP grid scale SM is assumed to be the weighted average of SM with and without canopy cover using the corresponding soil emissivity e_s by the fractional cover. The MEP retrievals of e_s(~0.8–0.9) captures the seasonality and variation of the SMAP data (Figure 7). Higher MEP e_s than the SMAP retrievals at the core sites is consistent with that at the temperal forest sites (Figures 2b and 2c). The MEP SM retrievals (Figure 9) are in reasonable agreement with the SMAP data and in situ observations characterized by high correlations (0.74–0.91 in Table 2).

The MEP retrievals of γ also captures the seasonality of the SMAP data (Figure 8). Higher MEP γ(>0.9) at the core sites than that at the forest sites ($\gamma \sim 0.7$ in Figure 3) is caused by lower VWC of grassl and crop canopy than that of forest canopy and the difference between the b coefficients of the MEP and SMAP τ-VWC relationship (see previous discussion). The MEP retrievals of VWC (~1 kg m^{-2}) are consistent with the SMAP ancillary data at Little Washita and TxSON site (Figures 10a and 10b). The MEP VWC at Little River site (Figure 10c) has the same seasonality as the SMAP ancillary data (~3 kg m^{-2}) with lower values (~1 kg m^{-2}). The difference is arguably caused by the physical parameters (e.g., $\rho_s c_s \delta_s$, $\rho_v c_v \delta_v$ in Equation 8). Due to the range and uncertainty of δ_s,δ_v (Table 1) for the dry biomass at the core sites including Little River site, $\rho_v c_v \delta_v \sim 0.3$(J m^{-2} C^{-1}) used in this proof-of-concept analysis for the three core sites may lead to lower MEP VWC compared to the SMAP ancillary data. Closer agreement between the MEP and SMAP VWC is expected to obtain when more accurate vegetation

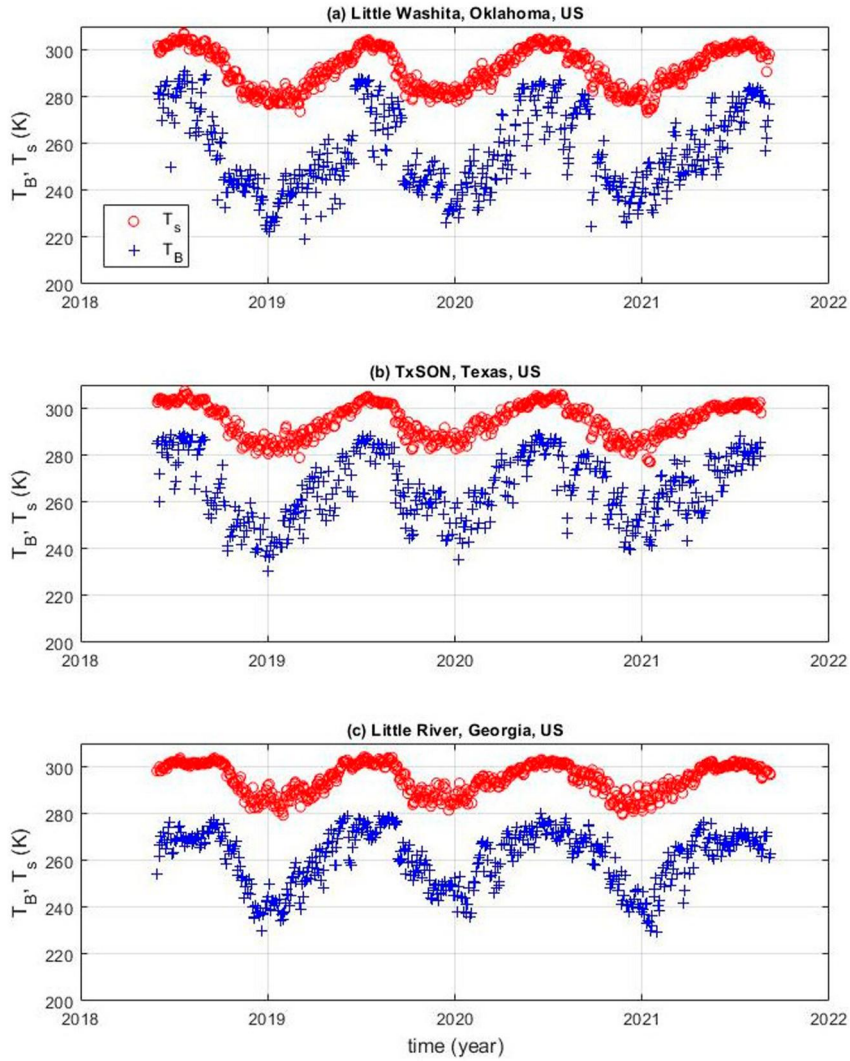

Figure 6. The input of the MEP algorithm from the SMAP V-polarized L-band brightness temperature T_B and the SMAP ancillary data of surface temperature T_s at the three SMAP core validation sites.

parameters are available if the SMAP ancillary VWC data are accurate. Nonetheless, the MEP algorithm with realistic physical parameters is able to retrieve low VWC (<5 kg m^{-2}) of grassland and cropland.

4.2. Discussion

As explained in the Introduction with details in Appendix A, Ohm's law has two equivalent representations in the forms of the principle of minimum dissipation and the principle of maximum entropy production for electromagnetic wave propagation in conductive materials. The proposed MEP theory as the theoretical foundation of the MEP algorithm of simultaneous retrieval of SM and WVC expounded in this report may be viewed as the counterpart of Ohm's law, represented by the principle of minimum dissipation, for electromagnetic wave propagation in dielectric materials. It is unclear whether the principle of minimum dissipation for dielectric materials has a representation in the form of Ohm's law (i.e., relating voltage, current and resistance). If (microwave) radiative flux through the materials, for example, canopy, is an analogy of electric current and the radiative inertia introduced in this study is an analogy of resistance, the analogy of voltage is yet to be defined. Nonetheless, the proposed formula of the dissipation function in Equation 3 is shown to be what is needed for formulating the simultaneous retrieval algorithm of SM and VWC from a single polarization of L-band TB. Just like Ohm's Law solves the electromagnetic wave transfer in conductive materials without explicitly solving Maxwell's equations, the MEP algorithm solves the radiative transfer in dielectric materials without explicitly

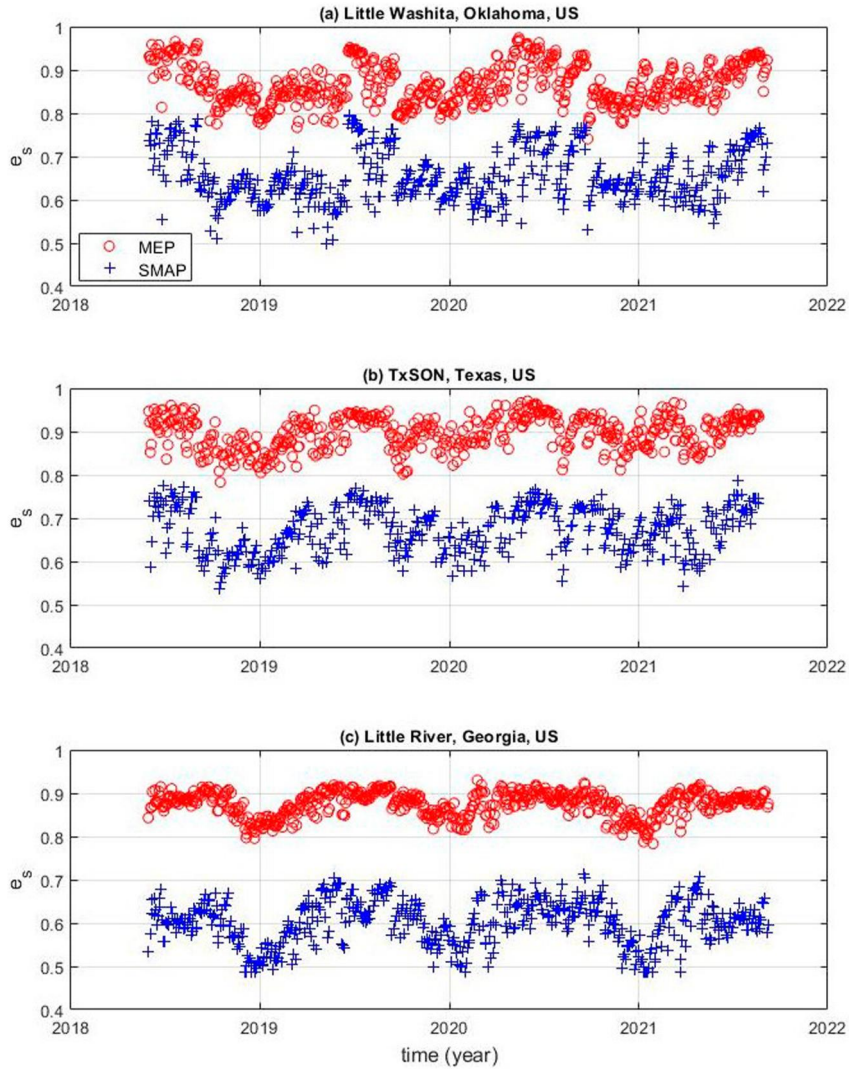

Figure 7. The MEP retrieval of surface emissivity e_s in Equation 9 using the input data shown in Figure 6 at the three SMAP core validation sites.

solving the radiative transfer equations or Maxwell's equations. The forward method through solving the radiative transfer model for the retrievals of SM and VWC needs more information about the canopy structures (e.g., leaf shape, size, vertical distribution, etc.) while the inverse method (e.g., the MEP algorithm) directly relates the variables of interest (e.g., SM and VWC) to the observables (brightness and physical temperature).

The MEP retrievals of SM and VWC (Figures 2–5 and 7–10) are based on the classical tau-omega (or integrated radiative transfer) model in Equation 1 for describing the electromagnetic wave propagation through canopy. Improved descriptions of radiative transfer through canopy (e.g., Colliander et al., 2020) may replace Equation 1 for potential improvement of the MEP retrievals of SM and VWC. The effect of non-uniform canopy temperature may also be taken into account in the tau-omega model to further improve the representation of radiative transfer through canopy. Improvement of the MEP algorithm is expected with surface temperature used in this proof-of-concept analysis replaced by effective temperature (e.g., Choudhury et al., 1982) to obtain a more accurate parameterization of microwave radiation from the soil. An analytical model (Lu et al., 2014) allows the derivation of soil temperature profile from the time-series record of surface temperature to avoid under-canopy soil temperature profile data. More improvement may also be achieved by taking sub-grid variability of VWC (e.g., foliage vs. trunk) into account in the tau-omega models as SMAP L-band TB has relatively coarse resolution (~40 km). The grid averaged physical parameters in the MEP algorithm such as penetration depth of vegetation

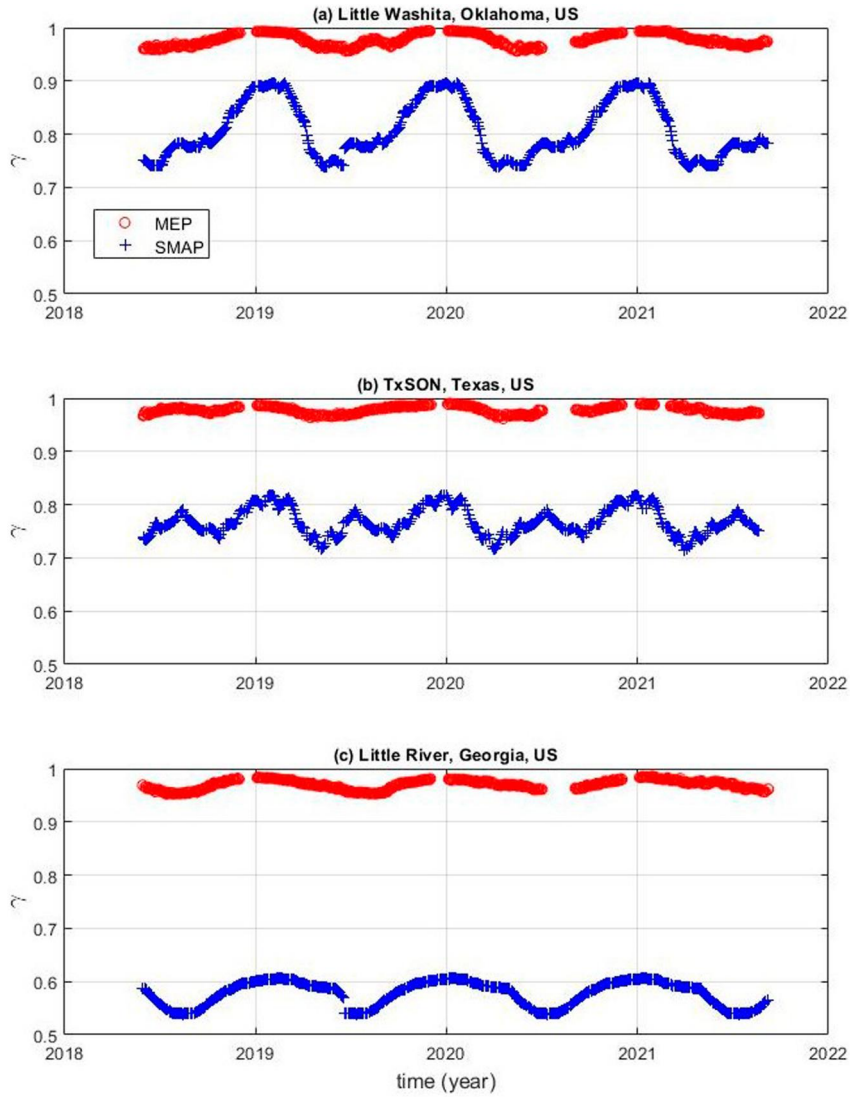

Figure 8. The MEP retrieval of canopy transmissivity γ in Equation 9 using the input data shown in Figure 6 at the three SMAP core validation sites.

materials may be calculated from the probability distribution of foliage and trunk for the MEP retrievals of grid averaged SM and VWC.

The proof-of-concept tests justify more applications of the MEP algorithm to a broad range of vegetation types globally since the MEP theory is a general (physical) principle applicable to all ecosystems. The MEP algorithm only including physical parameters facilitates the global retrievals of SM and VWC while the current retrieval algorithms use empirical parameters (e.g., b in $\tau = b \times VWC$) that need calibration using location specific data. The MEP algorithm using a small number of physical parameters has the potential to reduce the biases and uncertainties of the SM and VWC retrievals. The number of the MEP algorithm parameters will be further reduced when a MEP algorithm of direct SM retrieval is formulated without using the dielectric mixing model in this proof-of-concept analysis. Theoretically, the MEP algorithm is applicable to SM and VWC retrievals from both vertically and horizontally polarized TB. In a follow-up study, a MEP algorithm of SM directly derived from the MEP retrieval of soil emissivity will be formulated without using dielectric mixing model(s). The MEP algorithm can be implemented in the SMAP SM retrieval system since the MEP algorithm input is a subset of that required by the current SMAP SM retrieval algorithms. Development of the MEP algorithms for the operational

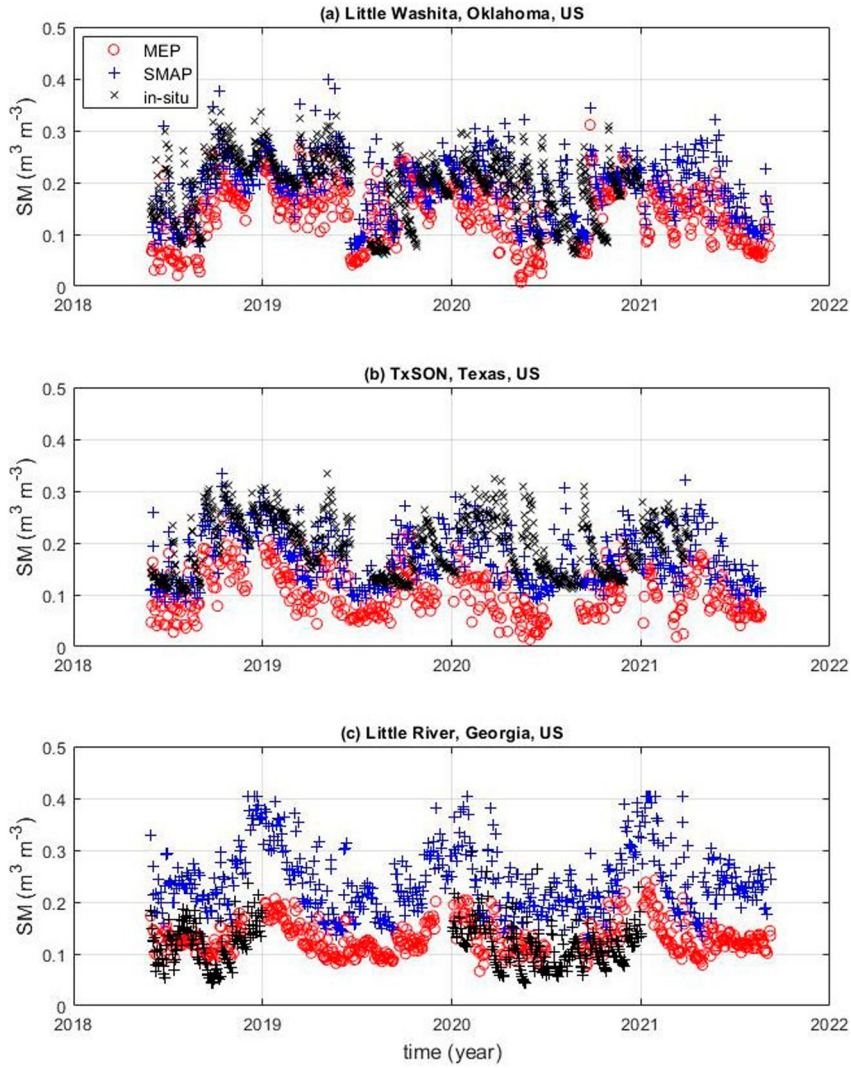

Figure 9. The MEP retrieval of soil moisture (SM) using the SMAP single channel algorithm (SCA) and the MEP e_s shown in Figure 7.

production of remote sensing data of SM and VWC needs more accurate estimates of vegetation and soil parameters including density, specific heat and complex dielectric constant.

The application of the MEP theory of electromagnetic wave propagation in terms of the principle of minimum dissipation is not limited to L-band frequency. In principle, the MEP theory is applicable to the full spectrum of electromagnetic radiation in dielectric materials. It not only opens new opportunities for SM and VWC retrieval from a broader spectrum of microwave radiometry but also broadens the applications of the L-band microwave radiometry to remote sensing of the Earth system beyond SM and VWC.

Table 3 compares the SMAP, SMOS and MEP algorithms of SM and VWC retrieval highlighting the new contribution of this study: retrieval of SM under dense canopy (VWC >5 kg m^{-2}) and VWC from L-band radiometry,

5. Conclusions

- The theory of maximum entropy production (MEP) for electromagnetic wave propagation in dielectric materials is proposed as an analogy of Ohm's law for conductors. The MEP theory in the form of the principle of minimum dissipation holds for all frequencies of electromagnetic waves in dielectric materials.

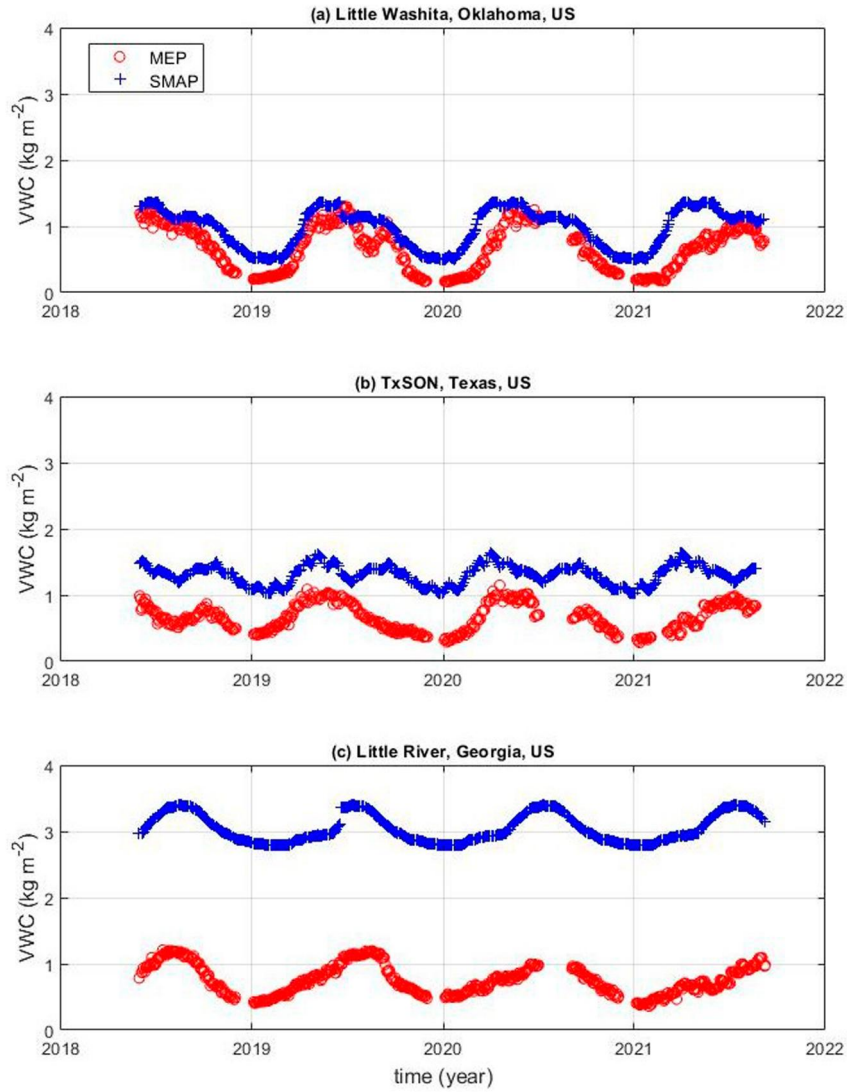

Figure 10. The MEP retrieval of vegetation water content VWC in Equation 13 derived from the MEP γ shown in Figure 8.

- An algorithm of simultaneous retrieval of SM and VWC from a single polarization of L-band brightness temperature based on the MEP theory is formulated and tested. The MEP algorithm is made possible by introducing new physical parameters (i.e., radiative diffusivity and radiative inertia) in terms of complex dielectric constant and heat capacity of the material. The MEP algorithm does not use empirical parameters.

Table 3
ARTE—Aggregated Radiative Transfer Equation; SM—Surface Soil Moisture; VWC—Vegetation Water Content; TB—Brightness Temperature; VOD—Vegetation Optical Depth Equation 11

Study	Method	Input	Output
1. SMAP	ARTE ($\tau - \omega$ model)	L-band TB	SM
Entekhabi et al. (2010)		Surface/canopy temperature	
O'Neill, Bindlish, et al. (2020)		Canopy VOD	(VWC <5 kg m^{-2})
2. SMOS	ARTE ($\tau - \omega$ model)	same as above	
Kerr et al. (2010, 2012)			
3. MEP	Dissipation function	L-band TB	SM, VWC
This study	Minimization	Surface/canopy temperature	(any VWC)

- The MEP algorithm allows the retrieval of SM under dense canopy of $VWC > 5$ kg m^{-2}.

Appendix A: Equivalent Representations of Ohm's Law

Ohm's law is equivalent to two physical principles: the principle of minimum dissipation and the principle of maximum entropy production.

1. The principle of minimum dissipation

Consider two parallel resistors with resistance R_1, R_2, respectively. The thermal dissipation D produced by electric currents through the resistors I_1, I_2 is expressed as,

$$D = \frac{I_1^2}{R_1} + \frac{I_2^2}{R_2}. \tag{A1}$$

I_1, I_2 under the constraint of given total current $I_0 = I_1 + I_2$ can be obtained from,

$$\min_{\{I_1, I_2\}} \{D | I_1 + I_2 = I_0\}, \tag{A2}$$

leading to,

$$\frac{I_1}{R_1^{-1}} = \frac{I_2}{R_2^{-1}} = V_0 \tag{A3}$$

where V_0 is voltage. (A3) recognized as the Ohm's law is equivalent to minimum (thermal) dissipation produced by electric current through resistor under the constraint of given total current. The voltage is recognized as the Lagrange multiplier when solving the constrained minimization problem in Equation A2. The minimized dissipation function D_{min} is expressed as,

$$D_{\min} \equiv \min_{\{I_1, I_2\}} \{D | I_1 + I_2 = I_0\} = \frac{I_0^2}{R_1^{-1} + R_2^{-1}}. \tag{A4}$$

2. The principle of maximum entropy production

An entropy production function S for electric currents through two parallel resistors under isothermal condition is defined,

$$\dot{S} = \frac{I_1}{T_1} + \frac{I_2}{T_2}, T_1 = T_2 = T_0. \tag{A5}$$

I_1, I_2 under the constraint of given total thermal dissipation $D_0 = I_1^2 R_1 + I_2^2 R_2$ can be obtained from,

$$\max_{\{I_1, I_2\}} \left\{ \dot{S} \middle| I_1^2 R_1 + I_2^2 R_2 = D_0 \right\}, \tag{A6}$$

leading to,

$$\frac{I_1}{R_1^{-1}} = \frac{I_2}{R_2^{-1}} = V_0. \tag{A7}$$

Equation A7 again recognized as the Ohm's law is equivalent to maximum entropy production under the constraint of total thermal dissipation. The maximized entropy production S_{max} is expressed as,

$$\dot{S}_{\max} \equiv \max_{\{I_1, I_2\}} \left\{ \dot{S} \middle| I_1^2 R_1 + I_2^2 R_2 = D_0 \right\} = \frac{\sqrt{\left(R_1^{-1} + R_2^{-1}\right) D_0}}{T_0}. \tag{A8}$$

Data Availability Statement

The publicly available data sets used in this study include SMAP L3 products of L-band brightness temperature and soil moisture and ancillary data of surface and canopy temperature, vegetation water content, etc (O'Neill et al., 2021), in situ data of soil moisture at Tambopata, Peru (Negrón-Juárez et al., 2023; Wang, Cho, et al., 2023), in situ data of soil moisture and rainfall at the two US sites from AmeriFlux network (NEON, 2022; Wood & Gu, 2021), remote sensing rainfall data of Global Precipitation Measurement (GPM) IMERG product (Huffman et al., 2019), and Enhanced Vegetation Index (EVI) data of MODIS Terra (Vermote & Wolfe, 2015). Version 1.1 daily 300 m FCOVER products are available at https://land.copernicus.eu/global/products/fcover.

Acknowledgments
This study is funded by NASA SMAP project 80HQTR21T0064. A partial contribution to this work was made at Jet Propulsion Laboratory, California Institute of Technology under a contract with the National Aeronautics and Space Administration. The Tambopata site is funded by CONCYTEC-World Bank Grants 057-2018-FONDECYT-BM-IADT-MU and 011-2019-FONDECYT-BM-INC-INV.

References

Aviabile, V., Herold, M., Heuvelink, G. B. M., Lewis, S. L., Phillips, O. L., Asner, G. P., et al. (2016). An integrated pan-tropical biomass map using multiple reference datasets. *Global Change Biology*, *22*(4), 1406–1420. https://doi.org/10.1111/gcb.13139

Ayres, E., Colliander, A., Cosh, M. H., Roberti, J. A., Simkin, S., & Genazzio, M. A. (2021). Validation of SMAP soil moisture at terrestrial national ecological observatory network (NEON) sites show potential for soil moisture retrieval in forested areas. *Ieee Journal of Selected Topics in Applied Earth Observations and Remote Sensing*, *14*, 10903–10918. https://doi.org/10.1109/JSTARS.2021.3121206

Blackard, J. A., Finco, M. v., Helmer, E. H., Holden, G. R., Hoppus, M. L., Jacobs, D. M., et al. (2006). Mapping U.S. forest biomass using nationwide forest inventory data and moderate resolution information. *Remote Sensing of Environment*, *12*(4), 1658–1677. https://doi.org/10.1016/J.RSE.2007.08.021

Camacho, F., Sánchez, J., & Latorre, C. (2016). GIO global land component – Lot I "operation of the global land component", quality assessment report LAI, FAPAR, FCover Collection 300 m. Version 1, issue I1.10, Tech. Rep., GIO-GL Lot1 Consortium.

Chan, S., Bindlish, R., Hunt, R., Jackson, T., & Kimball, J. (2013). *Ancillary data report - vegetation water content, JPL D-53061*. Jet Propulsion Laboratory. Retrieved from http://smap.jpl.nasa.gov/science/dataproducts/ATBD/

Chan, S., Bindlish, R., O'Neill, P., Njoku, E., Jackson, T., Colliander, A., et al. (2016). Assessment of the SMAP level 2 passive soil moisture product. *IEEE Transactions on Geoscience and Remote Sensing*, *54*(8), 4994–5007. https://doi.org/10.1109/TGRS.2016.2561938

Chaubell, J., Simon, Y., Dunbar, R. S., Colliander, A., Entekhabi, D., Chan, S. K., et al. (2022). Regularized dual-Channel Algorithm for the retrieval of soil moisture and vegetation optical depth from SMAP measurements. *Ieee Journal of Selected Topics in Applied Earth Observations and Remote Sensing*, *15*, 102–114. https://doi.org/10.1109/JSTARS.2021.3123932

Cho, K., Negrón-Juárez, R., Colliander, A., Cosio, E., Salinas, N., de Araujo, A., & Wang, J. (2024). Calibration of the SMAP soil moisture retrieval algorithm to reduce bias over the Amazon rainforest. *IEEE Applied Earth Observations and Remote Sensing*. in revision. https://doi.org/10.5281/zenodo.8350626

Choudhury, B. J., Schmugge, T. J., & Mo, T. (1982). A parameterization of effective soil temperature for microwave emission. *Journal of Geophysical Research*, *87*(C2), 1301–1304. https://doi.org/10.1029/JC087iC02p01301

Colliander, A., Asanuma, J., Berg, A., Bongiovanni, T., Bosch, D., Caldwell, T., et al. (2017). *SMAP/In situ core validation site land surface parameters match-up data, version 1. [SMAPL2SMPE_ T17350]*. NASA National Snow and Ice Data Center Distributed Active Archive Center. https://doi.org/10.5067/DXAVIXLY18KM

Colliander, A., Cosh, M. H., Berg, A., Misral, S., Thomas, J., Bourgeau-Chavez, L., et al. (2022a). In *Development of SMAP Retrievals for Forested Regions: SMAPVEX19-22 and SMAPVEX22-Boreal, IGARSS 2022 - 2022 IEEE International Geoscience and Remote Sensing Symposium* (pp. 4228–4231). Kuala Lumpur. https://doi.org/10.1109/IGARSS46834.2022.9884441

Colliander, A., Cosh, M. H., Kelly, V. R., Kraatz, S., Bourgeau-Chavez, L., Siqueira, P., et al. (2020). SMAP detects soil moisture under temperate forest canopies. *Geophysical Research Letters*, *47*(19), e2020GL089697. https://doi.org/10.1029/2020GL089697

Colliander, A., Njoku, E. G., Huang, H., & Tsang, L. (2018). Soil moisture retrieval using full wave simulations of 3-D Maxwell equations for compensating vegetation effects. In *IGARSS 2018—2018 IEEE International Geoscience and Remote Sensing Symposium* (pp. 1418–1421). https://doi.org/10.1109/IGARSS.2018.8517453

Colliander, A., Reichle, R. H., Crow, W. T., Cosh, M. H., Chen, F., Chan, S., et al. (2022). Validation of soil moisture data products from the NASA SMAP mission. *Ieee Journal of Selected Topics in Applied Earth Observations and Remote Sensing*, *15*, 364–391. https://doi.org/10.1109/JSTARS.2021.3124743

Colliander, A., Reichle, R. H., Crow, W. T., Cosh, M. H., Chen, F., Chan, S., et al. (2022b). Validation of soil moisture data products from the NASA SMAP mission. *Ieee Journal of Selected Topics in Applied Earth Observations and Remote Sensing*, *15*, 364–392. https://doi.org/10.1109/JSTARS.2021.3124743

Dewar, R. C. (2003). Information theory explanation of the fluctuation theorem, maximum entropy production and self-organized criticality in non-equilibrium stationary states. *Journal of Physics A: Mathematical and General*, *36*(3), 631–641. https://doi.org/10.1088/0305-4470/36/3/303

Dewar, R. C. (2005). Maximum entropy production and the fluctuation theorem. *Journal of Physics A: Mathematical and General*, *38*(21), L371–L381. https://doi.org/10.1088/0305-4470/38/21/L01

Dewar, R. C., & Maritan, A. (2013). A theoretical basis for maximum entropy production. In R. Dewar (Ed.), *Beyond the Second law: Entropy production and non-equilibrium systems* (pp. 49–71). Springer.

Dobson, M. C., Ulaby, F. T., Hallikainen, M. T., & El-Rayes, M. A. (1985). Microwave dielectric behavior of wet soil – Part II: Dielectric mixing models. *IEEE Transactions on Geoscience and Remote Sensing*, *GE-23*(1), 35–46. https://doi.org/10.1109/TGRS.1985.289498

El Rayes, M. A., & Ulaby, F. T. (1987). Microwave dielectric spectrum of vegetation-Part I: Experimental observations. *IEEE Transaction on Geoscience Remote Sensing, GE-*, *25*(5), 541–549. https://doi.org/10.1109/TGRS.1987.289832

El Sharif, H., Zhou, W., Ivanov, V., Sheshukov, A., Mazepa, V., & Wang, J. (2019). Surface energy budgets in Arctic permafrost areas during growing season. *Journal of Geophysical Research: Atmospheres*, *124*(13), 6999–7017. https://doi.org/10.1029/2019JD030650

Entekhabi, D., Njoku, E., O'Neill, P., Kellogg, K., Crow, W. T., Edelstein, W. N., et al. (2010). The soil moisture active passive (SMAP) mission. *Proceedings of the IEEE*, *98*(5), 704–716. https://doi.org/10.1109/JPROC.2010.2043918

Gu, L., Pallardy, S. G., Yang, B., Hosman, K. P., Mao, J., Ricciuto, D., et al. (2016). Testing a land model in ecosystem functional space via a comparison of observed and modeled eco-system flux responses to precipitation regimes and associated stresses in a Central U.S. forest. *Journal of Geophysical Research: Biogeosciences*, *121*(7), 1884–1902. https://doi.org/10.1002/2015JG003302

Gu, W., Tsang, L., Colliander, A., & Yueh, S. (2022). Multifrequency full-wave simulations of vegetation using a hybrid method. *IEEE Transactions on Microwave Theory and Techniques*, *70*(1), 275–328. https://doi.org/10.1109/ACCESS.2022.3211323

Hajji, I., Nadeau, D., Music, B., Anctil, F., & Wang, J. (2018). Application of the maximum entropy production model of evapotranspiration over partially vegetated water-limited land surfaces. *Journal of Hydrometeorology*, *19*(6), 989–1005. https://doi.org/10.1175/JHM-D-17-0133.1

Hajji, I., Nadeau, D. F., Music, B., Anctil, F., & Wang, J. (2021). Analysis of water vapor fluxes over a seasonal snowpack using the maximum entropy production model. *Journal of Geophysical Research: Atmospheres*, *126*(1), e2020JD033049. https://doi.org/10.1029/2020JD033049

Huete, A. R., Didan, K., Shimabukuro, Y. E., Ratana, P., Saleska, S. R., Hutyra, L. R., et al. (2006). Amazonrainforests green-up with sunlight in dry season. *Geophysical Research Letters*, *33*(6), L06405. https://doi.org/10.1029/2005GL025583

Huffman, G. J., Stocker, E. F., Bolvin, D. T., Nelkin, E. J., & Tan, J. (2019). GPM IMERG final precipitation L3 1 day 0.1 degree x 0.1 degree V06 [Dataset]. Greenbelt, MD, Goddard Earth Sciences Data and Information Services Center (GES DISC). https://doi.org/10.5067/GPM/IMERGDF/DAY/06

Isabelle, P.-E., Viens, L., Nadeau, D. F., Anctil, F., Wang, J., & Maheu, A. (2021). Sensitivity analysis of the maximum entropy production method to model evaporation in boreal and temperate forests. *Geophysical Research Letters*, *48*(13), e2020GL091919. https://doi.org/10.1029/2020GL091919

Jackson, T. (1993). III. Measuring surface soil moisture using passive microwave remote sensing. *Hydrological Processes*, *7*(2), 139–152. https://doi.org/10.1002/hyp.3360070205

Jackson, T. J., & Schmugge, T. J. (1991). Vegetation effects on the microwave emission from soils. *Remote Sensing of Environment*, *36*(3), 203–212. https://doi.org/10.1016/0034-4257(91)90057-D

Jayalakshmy, M. S., & Philip, J. (2010). Thermophysical properties of plant leaves and their influence on the environment temperature. *International Journal of Thermophysics*, *31*(11–12), 2295–2304. https://doi.org/10.1007/s10765-010-0877-7

Jaynes, E. T. (1957). Information theory and statistics mechanics. *Physical Review*, *106*(4), 620–630. https://doi.org/10.1103/PhysRev.106.620

Jaynes, E. T. (2003). *Probability theory—The logic of science* (p. 755pp). Cambridge University Press.

Jeong, J., Tsang, L., Gu, W., Colliander, A., & Yueh, S. H. (2023). Wave propagation in vegetation field by combining fast multiple scattering theory and numerical electromagnetics in a hybrid method. *IEEE Transactions on Antennas and Propagation*, *71*(4), 3598–3610. https://doi.org/10.1109/TAP.2023.3242418

Jia, C., Zhao, P., Wang, J., Deng, Y., Li, N., Wang, Y., & Miao, S. (2023). An application of the maximum entropy production method in the WRF Noah land surface model. *Journal of Geophysical Research: Atmospheres*, *128*(5), e2022JD037867. https://doi.org/10.1029/2022JD037867

Jing, W., & Wang, J. (2023). A dynamics of surface temperature forced by solar radiation. *Geophysical Research Letters*, *50*(3), e2022GL101222. https://doi.org/10.1029/2022GL101222

Juretic, D., & Zupanovic, P. (2003). Photosynthetic models with maximum entropy production in irreversible charge transfer steps. *Computational Biology and Chemistry*, *27*(6), 541–553. https://doi.org/10.1016/j.compbiolchem.2003.09.001

Kerr, Y., Waldteufel, P., Richaume, P., Wigneron, J. P., Ferrazzoli, P., Mahmoodi, A., et al. (2012). The SMOS soil moisture retrieval algorithm. *IEEE Transactions on Geoscience and Remote Sensing*, *50*(5), 1384–1403. https://doi.org/10.1109/TGRS.2012.2184548

Kerr, Y. H., Waldteufel, P., Wigneron, J., Delwart, S., Cabot, F., Boutin, J., et al. (2010). The SMOS mission: New tool for monitoring key elements of the global water cycle. *Proceedings of the IEEE*, *98*(5), 666–687. https://doi.org/10.1109/JPROC.2010.2043032

Kleidon, A., & Fraedrich, K. (2005). Biotic entropy production and global atmosphere-biosphere interaction. In *Non-equilibrium thermodynamics and the production of entropy* (pp. 173–189). Springer.

Kleidon, A., & Lorenz, R. D. (2005). *Non-equilibrium thermodynamics and the production of entropy* (p. 260). Springer.

Kleidon, A., Malhi, Y., & Cox, P. M. (2010). Maximum entropy production in ecological environmental systems: Applications and implications. *Philosophical Transactions of the Royal Society B*, *365*, 1295–1455. https://doi.org/10.1098/rstb.2010.0018

Kleidon, A., & Schymanski, S. (2008). Thermodynamics and optimality of the water budget on land. *Geophysical Research Letters*, *35*(20), L20404. https://doi.org/10.1029/2008GL035393

Le Vine, D. M., & Karam, M. A. (1996). Dependence of attenuation in a vegetation canopy on frequency and plant water content. *IEEE Transactions on Geoscience and Remote Sensing*, *34*(5), 1090–1096. https://doi.org/10.1109/36.536525

Liu, X., Conner, W. H., Song, B., & Jayakaran, A. D. (2017). Forest composition and growth in a freshwater forested wetland community across a salinity gradient in South Carolina, USA. *Forest Ecology and Management*, *389*, 211–219. https://doi.org/10.1016/j.foreco.2016.12.022

Lu, P., Liu, Y., & Hiyama, T. (2014). Linking surface temperature based approaches for estimating soil heat flux with error propagation. *Atmospheric and Climate Sciences*, *4*(01), 29–41. https://doi.org/10.4236/acs.2014.41004

Lu, Y., Sloan, B., Thompson, S. E., Konings, A. G., Bohrer, G., Matheny, A., & Feng, X. (2022). Intra-specific variability in plant hydraulic parameters inferred from model inversion of sap flux data. *Journal of Geophysical Research: Biogeosciences*, *127*(6), e2021JG006777. https://doi.org/10.1029/2021JG006777

Mätzler, C. (1994). Microwave (1-100 GHz) dielectric model of leaves. *IEEE Transactions on Geoscience and Remote Sensing*, *32*(4), 947–949. https://doi.org/10.1109/36.298024

Mironov, V. L., Kosolapova, L. G., & Fomin, S. V. (2009). Physically and mineralogically based spectroscopic dielectric model for moist soils. *IEEE Transactions on Geoscience and Remote Sensing*, *47*(7), 2059–2070. https://doi.org/10.1109/TGRS.2008.2011631

Mo, T., Choudhury, B. J., Schmugge, T. J., Wang, J. R., & Jackson, T. J. (1982). A model for microwave emission from vegetation-covered fields. *Journal of Geophysical Research*, *87*(C13), 11229–11237. https://doi.org/10.1029/JC087iC13p11229

Nearing, S. G., Moran, M. S., Scott, R. L., & Ponce-Campos, G. (2012). Coupling diffusion and maximum entropy models to estimate thermal inertia. *Remote Sensing of Environment*, *119*, 222–231. https://doi.org/10.1016/j.rse.2011.12.012

Negrón-Juárez, R. I., Cho, K., Colliander, A., & Wang, J. (2023). In situ soil moisture measurement at Tambopata, Peru [Dataset]. Zenodo. https://doi.org/10.5281/zenodo.8350666

Negrón-Juárez, R. I., Hodnett, M. G., Fu, R., Goulden, M. L., & von Randow, C. (2007). Control of dry season evapotranspiration over the amazonian forest as inferred from observations at a Southern Amazon forest site. *Journal of Climate*, *20*(11), 2827–2839. https://doi.org/10.1175/JCLI4184.1

NEON (2022). AmeriFlux FLUXNET-1F US-xBR NEON (national ecological observatory network) [Dataset]. Bartlett Experimental Forest (BART), Ver. 3-5, AmeriFlux AMP. https://doi.org/10.17190/AMF/1881598

Njoku, E. G. (Ed.) (2014). *Encyclopedia of remote sensing*. https://doi.org/10.1007/978-0-387-36699-9

Njoku, E. G., & Kong, J.-A. (1977). Theory for Passive microwave remote sensing of near-surface soil moisture. *Journal of Geophysical Research*, *82*(20), 3108–3118. https://doi.org/10.1029/JB082i020p03108

Njoku, N. G., & Entekhabi, D. (1996). Passive microwave remote sensing of soil moisture. *Journal of Hydrology*, *184*(1–2), 101–129. https://doi.org/10.1016/0022-1694(95)02970-2

O'Neill, P., Bindlish, R., Chan, S., Chaubell, J., Njoku, E., & Jackson, T. (2020). *Algorithm theoretical basis document level 2 & 3 soil moisture (passive) data products, JPL D-66480*. Jet Propulsion Laboratory. Retrieved from https://nsidc.org/data/smap/technical-references

O'Neill, P., Chan, S., Bindlish, R., Chaubell, M., Colliander, A., Chen, F., et al. (2020). *Calibration and validation for the L2/3_SM_P version 7 and L2/3_SM_P_E version 4 data products, SMAP project, JPL D-56297*. Jet Propulsion Laboratory. Retrieved from https://pdms.jpl.nasa.gov/

O'Neill, P. E., Chan, S., Njoku, E. G., Jackson, T., Bindlish, R., Chaubell, J., & Colliander, A. (2021). SMAP enhanced L3 radiometer global and polar grid daily 9 km EASE-grid soil moisture version 5 [Dataset]. Boulder, Colorado USA. NASA National Snow and Ice Data Center Distributed Active Archive Center. https://doi.org/10.5067/4DQ54OUIJ9DL

Pallqui, N. C., Monteagudo, A., Phillips, O. L., Lopez-Gonzalez, G., Cruz, L., Galiano, W., et al. (2014). Dynamics, aboveground biomass and composition on permanent plots, Tambopata National Reserve. Madre de Dios. *Peru, Revista peruana de biología*, *21*(3), 235–242. https://doi.org/10.15381/rpb.v21i3.10897

Paltridge, G. W. (1975). Global dynamics and climate - a system of minimum entropy exchange. *Quarterly Journal of the Royal Meteorological Society*, *101*(429), 475–484. https://doi.org/10.1002/qj.49710142906

Reul, N., & Chapron, B. (2001). Smos - salinity data processing study - improvements in emissivity models (WP 1100 report). In *CLS/IFREMER/NERSC study*. ESA contract N°15165/01/NL/SF.

Shanafield, M., Cook, P. G., Gutiérrez-Jurado, H. A., Faux, R., Cleverly, J., & Eamus, D. (2015). Field comparison of methods for estimating groundwater discharge by evaporation and evapotranspiration in an arid-zone playa. *Journal of Hydrology*, *527*, 1073–1083. https://doi.org/10.1016/j.jhydrol.2015.06.003

Shipley, B. (2010). *From plant traits to vegetation structure – Chance and selection in the assembly of ecological communities* (p. 277). Cambridge University Press.

Shipley, B., & Vu, T.-T. (2002). Dry matter content as a measure of dry matter concentration in plants and their parts. *New Phytologist*, *153*(2), 359–364. https://doi.org/10.1046/j.0028-646X.2001.00320.x

Sims, D. A., Rahman, A. F., Cordova, V. D., El-Masri, B. Z., Baldocchi, D. D., Flanagan, L. B., et al. (2006). On the use of MODIS EVI to assess gross primary productivity of North American ecosystems. *Journal of Geophysical Research*, *111*(G4), G04015. https://doi.org/10.1029/2006JG000162

SMAP Algorithm Development Team. (2015). *Ancillary data report surface temperature version 2, JPL D-53064*. Jet Propulsion Laboratory. Retrieved from http://smap.jpl.nasa.gov/science/dataproducts/ATBD/

Tang, Y., Shahnaz, S., & Wang, J. (2021). A non-gradient model of turbulent gas fluxes over land surfaces. *Journal of Geophysical Research – Atmospheres*, *126*(14), e2021JD034605. https://doi.org/10.1029/2021JD034605

Torgovnikov, G. I. (1993). *Dielectric properties of Wood and wood-based materials*. Springer-Verlag.

Ulaby, F. T., Moore, R. K., & Fung, A. K. (1982). *Microwave remote sensing. Active and passive. Vol. 2. Radar remote sensing and surface scattering and emission*. Artech House.

Ulaby, F. T., Moore, R. K., & Fung, A. K. (1986). *Microwave remote sensing. Active and passive. Vol. 3. From theory to applications*. Artech House.

Vermote, E., & Wolfe, R. (2015). MOD09GA MODIS/Terra surface Reflectance daily L2G global 1kmand 500m SIN grid V006 [Dataset]. NASA EOSDIS Land Processes Distributed Active Archive Center. https://doi.org/10.5067/MODIS/MOD09GA.006

Vittucci, V., Ferrazzoli, P., Kerr, Y., Richaume, P., Guerriero, L., Rahmoune, R., & Laurin, V. (2016). SMOS retrieval over forests: Exploitation of optical depth and tests of soil moisture estimates. *Remote Sensing of Environment*, *180*, 115–127. https://doi.org/10.1016/j.rse.2016.03.004

Wang, H., Tetzlaff, D., & Soulsby, C. (2017). Testing the maximum entropy production approach for estimating evapotranspiration from closed canopy shrubland in a low-energy humid environment. *Hydrological Processes*, *31*(25), 4613–4621. https://doi.org/10.1002/hyp.11363

Wang, J., & Bras, R. L. (2009). A model of surface heat fluxes based on the theory of maximum entropy production. *Water Resources Research*, *45*(11), W11422. https://doi.org/10.1029/2009WR007900

Wang, J., & Bras, R. L. (2011). A model of evapotranspiration based on the theory of maximum entropy production. *Water Resources Research*, *47*(3), W03521. https://doi.org/10.1029/2010WR009392

Wang, J., Bras, R. L., Nieves, V., & Deng, Y. (2014). A model of energy budgets over water, snow and ice surfaces. *Journal of Geophysical Research - Atmospheres*, *119*(10), 6034–6051. https://doi.org/10.1002/2013JD021150

Wang, J., Cho, K., Negron-Juarez, R., & Colliander, A. (2023). A theory of maximum entropy production and its application to microwave remote sensing - simultaneous retrieval of soil moisture and vegetation water content [Dataset]. Zenodo. https://doi.org/10.5281/zenodo.7802217

Wang, J., Liu, H., & Shen, L. (2023). An observational and modeling study of inverse-temperature layer and water surface heat flux. *Geophysical Research Letters*, *50*(16), e2023GL104358. https://doi.org/10.1029/2023GL104358

Wang, J. R., & Schmugge, T. J. (1980). An empirical model for the complex dielectric permittivity of soils as a function of water content. *IEEE Transactions on Geoscience and Remote Sensing*, *18*(4), 288–295. https://doi.org/10.1007/s11707-009-0023-7

Wegmuller, U., Mätzler, C., & Njoku, E. G. (1995). Canopy opacity models. In B. J. Choudhury, Y. H. Kerr, E. G. Njoku, & P. Pampaloni (Eds.), *Passive microwave remote sensing of land-atmosphere Interactions* (pp. 375–387). VSP Publishing.

Wood, J., & Gu, L. (2021). AmeriFlux FLUXNET-1F US-MOz Missouri Ozark site [Dataset]. AmeriFlux AMP. Ver. 3-5. https://doi.org/10.17190/AMF/1854370

Xu, D., Agee, E., Wang, J., & Ivanov, V. (2019). Estimation of evapotranspiration of Amazon rainforest using the maximum entropy production method. *Geophysical Research Letters*, *46*(3), 1402–1412. https://doi.org/10.1029/2018GL080907

Xu, D., Ivanov, V. Y., Agee, E., & Wang, J. (2023). Energy surplus and an atmosphere-land-surface "tug of war" control future evapotranspiration. *Geophysical Research Letters*, *50*(15), e2022GL102677. https://doi.org/10.1029/2022GL102677

Xu, J., Lai, D. Y., & Neogi, S. (2020). Effects of land use types on CH4 and CO2 production potentials in subtropical wetland soils. *Water*, *12*(7), 1856. https://doi.org/10.3390/w12071856

Yang, J., & Wang, Z.-H. (2014). Land surface energy partitioning revisited: A novel approach based on single depth soil measurement. *Geophysical Research Letters*, *41*(23), 8348–8358. https://doi.org/10.1002/2014GL062041

Yang, Y., Sun, S., Zhu, M., Wang, J., & Zhang, W. (2022). An R package of maximum entropy production model to estimate 41 years of global evapotranspiration. *Journal of Hydrology*, *614*, 128639. https://doi.org/10.1016/j.jhydrol.2022.128639

Zawislanski, P. T., Wobber, F., Williams, K. H., Roberts, J., Peterson, J. E., Jr., Majer, E. L., & Hubbard, S. S. (1997). Estimation of Permeable Pathways and water content using tomographic radar data. *The Leading Edge*, *16*(11), 1553–1720. https://doi.org/10.1190/1.1437539